

https://dspace.org/

Treatment delivery verification using a pelvic anthropormophic phantom

Mwale, Nsangu Augustine

2009-09-02T12:03:20Z
http://hdl.handle.net/10539/7173

Downloaded from a DSpace repository. https://dspace.org/

TREATMENT DELIVERY VERIFICATION USING A PELVIC ANTHROPORMOPHIC PHANTOM

Nsangu Augustine Mwale

A research report submitted to the Faculty of Science, University of the Witwatersrand, Johannesburg, in partial fulfillment of the requirements for the degree of Master of Science.

Johannesburg, 2009

DECLARATION

I declare that this research is my own, unaided work. It is submitted for the degree of Master of Science at the University of the Witwatersrand, Johannesburg. It has not been submitted before for any degree or examination in any other University.

_____

(Signature of candidate)

_____ day of _____2009

ABSTRACT

Aim: A series of measurements in a pelvic anthropomorphic phantom was performed as part of the validation of the entire radiotherapy treatment chain. Two treatment planning calculation algorithms were used: the Pencil Beam (PB) and the Collapsed Cone (CC). The dose calculation algorithms of Radiotherapy Treatment Planning Systems (RTPS) were validated to ensure that the dose delivered to a treatment target was accurately predicted. An anthropomorphic phantom, designed and manufactured locally at the Pretoria Academic Hospital, was employed in this study. The phantom was fabricated with locally available materials as human tissue substitutes based on the attenuation coefficients, electron densities and effective atomic numbers.

Materials: Pelvic anthropomorphic phantom, Thermoluminescent Dosimeters (TLD_100 chips), X-Omat V film, film processors, a densitometer and 6 MV and 15 MV linear accelerator photon beams with beam quality ($TPR_{20,10}$) of 0.674 and 0.763 respectively.

Results: Two treatment planning techniques were studied, a four field “box” and parallel opposed beams using a local cancer of the cervix protocol. Point doses calculated by the RTPS were compared with equivalent point dose values measured with thermoluminescent dosimeters (TLDs). Three dose regions emerged for the four field technique, those of low, intermediate and high dose gradient. The four field technique for 6 MV gave a dose deviation from -4.9% to -32.1% and at 15 MV from -1.5% to -20.6%. For 6 MV and 15 MV parallel opposed beams, percentage dose deviations from -2.7% to -11.8% and from +0.2% to -11.5 were observed. The mean value of the ratios of measured to calculated dose values was 0.91±0.05 for the four field technique and 0.94±0.02 for the AP/PA. Radiographic film was used to compare the predicted 2D isodose distributions to the actual dose distribution in the phantom. The 2D isodose distributions obtained were not meaningful in comparing the doses predicted by the planning system. A smaller field size of 7 cm x 7 cm was also employed and results of both TLD and film obtained were comparable to those predicted by the planning system.

Conclusion: The stated goal of dose delivery accuracy (ICRU, 1987) to within 5% was not generally met in this study. On average the measured doses using TLDs and film at a field size of 7 cm x 7 cm *were lower* than the point doses predicted by the RTPS dose calculation algorithms whereas the film *over-responded* when a local cancer of the cervix protocol was employed. At a field size of 7 cm x 7 cm, film dosimetry was comparable to the TLD results. Film and TLDs were calibrated perpendicularly and exposed parallel. The phantom is unsuitable for film dosimetry studies at field sizes more than 14 cm x 14 cm.

In Memory of my late parents,

Elson Joseph Mwale (1956 -1999) and Elizabeth Sakala Mwale (1956 -2000)

who made tremendous sacrifices to ensure that I had a good education, for this and much more, I am forever in their debt.

ACKNOWLEDGEMENTS

I would like to thank the International Atomic Energy Agency (I.A.E.A) for the financial support during my two year internship training at the Johannesburg Hospital, the Canon Collins Trust, my supervisor Professor Debbie Van Der Merwe for suggesting this work and helping with developing the treatment plans. I am grateful to The Division of Radiation Oncology, Johannesburg Hospital for making the equipment available for this experiment, to Prof A. J. Van Rensburg, Pretoria Academic Hospital for helping with the film scanner, to Nico Van Der Merwe for providing the densitometer, to Lindiwe for developing the cast, and the Johannesburg Hospital Radiation Oncology staff, who have been absolutely kind.

I would also like to thank my family for moral support, especially my brothers Steve and Chitalu, my sisters Ann and Linda. I love you. You are the semantics behind all that I do.

CONTENTS

ABSTRACT iii
ACKNOWLEDGEMENTS vi
LIST OF TABLES viii
LIST OF FIGURES ix
1.0 INTRODUCTION 1
1.1 Objectives/Rationale of Study 3
2.0 LITERATURE REVIEW 4
2.1 Interaction of photons with matter 4
2.1.1 Energy deposition by photon beams 5
2.1.2 Kerma 6
2.1.3 Absorbed dose 7
2.1.4 Primary and scattered dose components 7
2.2 Experimental quantities 7
2.3 Treatment planning system 8
2.3.1 Monitor Unit (MU) Calculation 10
2.4 Film dosimetry 11
2.5 Thermoluminescent dosimetry 14
2.6 Computed Tomography 17
2.7 The radiotherapy procedure 19
2.7.1 Beam combinations 19
2.7.2 Single photon beam 19
2.7.3 Parallel opposed beams 20
2.7.4 Four field “box” 20
2.7.5 Treatment verification 20
3.0 METHODOLOGY 22
3.1 Phantom fabrication 22
3.2 TLD Procedure 24
3.3 Calibration and irradiation process 24
3.4 Film calibration 27
3.5 Dose calculation on Helax-TMS 29
4.0 RESULTS 36
5.0 DISCUSSION 41
6.0 CONCLUSION AND RECOMMENDATIONS 44
REFERENCES 47
APPENDIX A 51
APPENDIX B 59

LIST OF TABLES

TABLE 3.1: Treatment protocol showing the number of MUs needed to deliver 0.7 Gy to the isocenter for no inhomogeneity, manual calculation, PB algorithm and CC algorithm.

TABLE A.1: Individual TLD results for 6 MV AP/PA compared to point doses predicted by the planning system when the local cancer of the cervix protocol is used.

TABLE A.2: Individual TLD results for 6 MV four field "box" compared to point doses predicted by the planning system when the local cancer of the cervix protocol is used.

TABLE A.3: Individual TLD results for 15 MV AP/PA compared to point doses predicted by the planning system when the local cancer of the cervix protocol is used.

TABLE A.4: Individual TLD results for 15 MV four field "box" compared to point doses predicted by the planning system when the local cancer of the cervix protocol is used.

TABLE A.5 Individual TLD and film results for 6 MV AP/PA treatment plan based on figure 4.9 compared to point doses predicted by the planning system.

TABLE A.6 Individual TLD and film results for 6 MV four field "box" treatment plan based on figure 4.10 compared to point doses predicted by the planning system.

TABLE B.1 This table shows Kanduza's results at 6 MV using the AP/PA technique Kanduza (2005).

LIST OF FIGURES

FIGURE 2.1	Gurney and Mott model of latent image. AgBr remains in the ionic form (Ag+Br−) in the crystal of the grain .Radiation produces ionization of Br− to Br_+e. These electrons make the speck negatively charged. The Ag+ migrate to neutralize the speck and forms a lump of Ag (aggregate) on the speck (Pai *et al*, 2007).
FIGURE 2.2	A simplified energy diagram to illustrate thermoluminescence process (Khan, 2003).
FIGURE 2.3	Diagram showing apparatus for measuring thermoluminescence (Khan, 2003).
FIGURE 3.1	Diagnostic imaging insert 1 (Kanduza, 2005).
FIGURE 3.2	Dosimetric insert 2 (Kanduza, 2005).
FIGURE 3.3	Position of film and TLDs in the dosimetric insert (Kanduza, 2005)
FIGURE 3.4	Variation of TLD output (Gy) with prescribed dose (Gy) at 6 MV. The error bars represent the overall deviation in the measurements
FIGURE 3.5	Variation of TLD output (Gy) with prescribed dose (Gy) at 15 MV. The error bars represent the overall deviation in the measurements.
FIGURE 3.6	Sensitometric curves at 6 MV and 15 MV for the perpendicular setup. The uncertainties were very small, hence error bars not visible.
FIGURE 3.7	Pencil Beam parallel opposed dose distribution at the level of the isocenter using 6 MV beams.
FIGURE 3.8	Collapsed Cone parallel opposed dose distribution at the level of the isocenter using 6 MV beams.
FIGURE 3.9	Pencil Beam parallel opposed dose distribution at the level of the isocenter using 15 MV beams.
FIGURE 3.10	Collapsed Cone parallel opposed dose distribution at the level of the isocenter using 15 MV beams.
FIGURE 3.11	Pencil Beam four field “box” dose distribution at the level of the isocenter and the position of the cut film using 6 MV Beams.

FIGURE 3.12 Collapsed Cone four field “box” dose distribution at the level of the isocenter using 6 MV beams.

FIGURE 3.13 Pencil Beam four field “box” dose distribution at the level of the isocenter using 6 MV beams.

FIGURE 3.14 Collapsed Cone four field “box” dose distribution at the level of the isocenter using 15 MV beams.

FIGURE 3.15 Pencil Beam parallel opposed dose distributions of a 7 x 7 cm field size at the level of the isocenter using 6 MV beams.

FIGURE 3.16 Pencil Beam four field “box” dose distributions (7 x 7 cm box) at the level of the isocenter using 6 MV beams.

FIGURE 4.1 The comparison between the dose measured by the TLD’s using the AP/PA technique to the dose calculated by the PB algorithm at 6 MV.

FIGURE 4.2 A comparison between the dose measured by the TLDs and that calculated by the PB algorithm using the four field “box” technique at 6 MV. Three dose regions emerged, those of low, intermediate and high dose gradient.

FIGURE 4.3 A comparison of measured dose with that calculated by the planning system for the AP/PA technique at 15 MV using TLDs. The PB algorithm was used to calculate dose.

FIGURE 4.4 A comparison between the dose measured by the TLDs and that calculated by the PB algorithm using the four field “box” technique at 15 MV. Three dose region emerged, those of low, intermediate and high dose gradients.

FIGURE 4.5 Ratio of measured to the calculated doses vs calculated doses for AP/PA at 6 MV using TLDs. The PB algorithm was used to calculate the doses.

FIGURE 4.6 Ratio of measured to the calculated doses vs calculated doses for the four field “box” at 6 MV using TLDs. The PB algorithm was used to calculate doses.

FIGURE 4.7 Ratio of measured to the calculated doses vs calculated doses for AP/PA at 15 MV using TLDs. The PB algorithm was used to calculate doses.

FIGURE 4.8 Ratio of measured to the calculated doses vs calculated doses for four field “box” at 15 MV using TLDs. The PB algorithm was used to calculate doses.

FIGURE A.1 Figure A.1 2-D isodose distribution at 15 MV for the four field box technique, film was cut and positioned as shown in figure 4.5

FIGURE A.2 Figure A.2 Shows an exposed film (using a 7 x 7 cm field size) at 6 MV for the four field box technique, film was cut and positioned figure 4.10.

1.0 INTRODUCTION

Radiation oncology is a clinical process that uses radiation for the treatment of cancer. The probability of success in radiotherapy with external photon beams depends strongly on delivering an adequately high dose to the intended target volume and at the same time, limiting dose to normal tissues close to the tumor (Delich *et al*, 1999). This results in the eradication of the disease, the propagation of life and/or the improvement in the quality of life. For some tumors and normal tissues, the response curve is very steep and a small change in dose can result in a large change in the probability of tumor control and normal tissue complications. This leads to strong demands on the accuracy in dose delivery. The International Commission on Radiation Units and Measurements (ICRU) (ICRU, 1987) has recommended that the dose must be delivered to within 5% of the treatment prescription. In order to satisfy this recommendation, each step involved in the radiotherapeutic process has to be performed at an accuracy better than 2% (ICRU, 1976). Other reviews have suggested accuracies in dose delivery of ±3.5% (Brahme, 1984). As part of the overall uncertainty arises from the process of dose calculations in treatment planning, the tolerances for the accuracy of a Radiotherapy Treatment Planning Systems (RTPS) have to be appropriately smaller (Mijnheer *et al*, 1987). To meet these delivery standards, quality assurance (QA) for RTPS is required. One of the most relevant parts of the RTPS QA is verification of the dose calculation.

An accurate knowledge of the distribution of the dose within patients undergoing external beam radiotherapy has been an essential requirement for the efficient planning and verification of treatment regimes for many years. As a result, many different materials have been used to simulate the body/ body sections during dose measurements involving therapeutic radiation beams. Modern treatment planning techniques use highly advanced tools to conform the dose distribution to the target, e.g., asymmetric beams, irregular beams shaped by multileaf collimators (MLC) and noncoplanar beams. A RTPS requires input of several physical and dosimetric data related to the radiotherapy treatment machine (Percentage Depth Dose (PDD) curves, off axis scans, etc) before actual use in patient treatment dosimetric evaluations. The RTPS has to be tested thoroughly by means

of both homogeneous and anthropomorphic phantoms, so that knowledge of the simulation capabilities of the computerized system can be obtained (Dunscombe *et al*, 1996). The testing procedure is mandatory because the accuracy in computing the dose distribution is influenced by the raw data describing the characteristics of the input radiation beams.

Ideally, confirmation of adequate performance of a RTPS should be based on the comparison of measured and calculated doses in patients receiving treatment as this is the situation for which the system is designed. In practice of course this is not feasible directly and validation has to rely on confirmation of the system's accuracy by comparing calculation and measurement under experimental conditions that, to a greater or lesser degree, reflect the clinical situation. Uncertainties in dose delivery may be introduced at the treatment phase (including machine calibration) or during the process of deriving monitor unit (MU) or timer settings from the dose prescription determined during treatment preparations. The latter type, arising at the treatment planning phase, could potentially affect the whole course of treatment and therefore are of particular concern. The MU settings required to deliver the prescribed dose are often calculated by a computerized treatment planning system using methods and quantities different from those in manual MU calculations. For computerized calculations of MU, whether or not accompanied by a dose distribution, uncertainties may be further categorized as arising from the input data, the calculation algorithm, incorrect use of the system or data transfer to the treatment sheet (Leszczynski and Dunscombe, 2000). MU calculations must also be compared with point/absolute dose (e.g. Gy) calculations as significant discrepancies of up to 5% have been observed (Starkschall *et al*, 2000). When comparing RTPS-calculated dose values with measured dose values, the discrepancies observed may be attributed to measurement error or to the RTPS calculation algorithms. Possible problems with the RTPS calculation include physical limitation of the beam model used in the dose-calculation matrix size, incorrect beam data and limitations in the computer code of the dose-calculating algorithm (Herrick *et al*, 1999).

There are several sources of uncertainties which affect the accuracy of planning and treatment. These are: (a) Patient localization, (b) Imaging, (c) Definition of anatomy, (d) Establishment of beam geometry (e) Dose calculations, (f) Dose display and plan evaluation, (g) Plan implementation, (h) Treatment delivery (Fraass *et al*, 1998).

In routine clinical practice, the more likely sources of systematic dose errors for individual patients result from misuse systems e.g. through inadequate understanding of normalization protocols, misinterpretation of the system output or data transfer errors (Leszczynski and Dunscombe, 2000).

1.1 Objectives/Rationale of Study

The high incidence of cervical cancer in sub-Saharan Africa has led to the need for a comprehensive set of quality assurance (QA) guidelines that can be applied to relatively simple clinical treatment planning. The aim of this study was to employ a pelvic anthropomorphic phantom (Kanduza, 2005) to verify the quality and consistency of treatments by mimicking the many steps involved in a radiotherapy process. The RTPS (Helax TMS, 2003) dose calculation algorithms were compared with measured doses in the pelvic anthropomorphic phantom for parallel opposed and four field “box” techniques at two different energies. Should this result contribute to verifying the overall integrity of the radiation therapy chain, a procedure could be developed for international dosimetry audits in developing countries for conventional techniques. The latter have to date, been restricted to absolute dosimetry protocols only.

2.0 LITERATURE REVIEW

2.1 Interaction of photons with matter

When a beam of photons enters a patient, energy is transferred from the beam and deposited within the patient as a result of photon interactions. Photon interaction in radiotherapy is dominated by three competing processes involving the atoms of the tissues: the photoelectric effect, the Compton effect and pair production. In water-like tissues with effective atomic number (Z_{eff}) of approximately 7.5, the probability of Compton events dominates (>80%) for energies between 0.05 MeV and 10 MeV thus the accurate modeling of Compton scattering events is an essential ingredient of any method of inhomogeneity correction for megavoltage photon beams. For higher atomic number materials, such as bone (Z_{eff}=13), the energy range of Compton dominance is reduced (0.08 to 7 MeV). The photoelectric effect depends on the photon energy and the atomic number (Z) of the material. The probability of a photoelectric interaction decreases as $(1/E_o^3)$ and Z^3. As a result the dose to bone relative to the dose to water will be increased, for a given photon fluence (Khan, 2003., Papanikalaou *et al,* 2004). The initial photon interactions within tissue are characterized by a linear attenuation coefficient (μ) which is the probability of a photon interacting per unit distance. The probability depends on: (a) the incident photon energy (MeV), (b) the tissue density (g/cm^3) and the (Z_{eff}) of the tissue (Khan, 2003).

The main aim of dosimetry in radiotherapy is "to measure or predict the absorbed dose in various tissues of a patient undergoing radiotherapy" (Metcalfe *et al*, 1997). This involves two steps: first, the assessment of the absorbed dose by a radiation detector in a suitable phantom and second, the use of beam and patient data such as tumor location and patient contours to predict dose at any point in the patient. It is generally assumed that a 5% difference in dose delivered to a patient does make a clinically detectable difference in treatment outcome (Metcalfe *et al*, 1997). For example an under dosage of a tumor by 5% may reduce the tumor control probability by more than 15% (Karzmark, 1993).

Absorbed dose is strictly defined as the mean energy imparted (by ionizing radiation) per mass (ICRU, 1998) i.e. dose is decoupled from the radiation used to deliver it. Therefore, absorbed dose is the fundamental physical quantity of interest for relating radiation treatment to its outcome. The broad spectrum of events that impart energy to matter implies that direct measurement of dose from its definition is not a trivial task. Calorimeters and ionization chambers can be used to measure dose in absolute terms but are not suitable for *in vivo* dosimetry. TLDs and diodes, placed on the patient's surface or within cavities, are used to check entrance or exit-dose measurements and the delivered dose within patients, but they are not suitable for obtaining an in-vivo map of the dose. Entrance dose measurements can provide confirmation of machine calibration and patient position relative to the accelerator, whilst exit dose measurements can also confirm beam alignment and the radiological thickness of the patient.

2.1.1 Energy deposition by photon beams

The photons from a treatment machine yield a cascade of interactions, not only in the patient but also in the treatment machine itself before the energy is absorbed as dose. Irradiation within the treatment head adds a secondary photon and electron component to the primary beam. As such the build up region is a contribution from contaminant charged particles in the treatment machine head and the air column between the head and the irradiated medium. Starting at the source (electron beam target), most photons entering the patient have not been subject to any interactions before entering the patient and will serve as the originators of the primary and phantom scatter dose distributions. Particles interacting in the treatment head yield two dose categories: charged particle contamination and head scatter dose. Head scatter dose accounts for approximately 5 – 15% of the total dose depending on the energy (Ahnesjo, 1994). The dosimetric data used in treatment planning are mainly derived from measurement in water. Fano's theorem states that when an object of varying density but constant atomic composition is exposed to a uniform photon fluence (under charged particle equilibrium (CPE)), differential in energy and direction, then the fluence of charged particles launched by the photons is also constant and independent of density variations (Fano, 1954). This constant fluence of

secondary electrons equals the fluence in CPE for a given fluence of photons. This implies that the absorbed dose across any area of density variation would be constant. Fano's theorem is an important test of dose calculation algorithms (Nilson and Knoos, 1992). To apply Fano's theorem to external radiation beams, the primary photon attenuation, stopping power density effect and release of secondary photons can be neglected in an equilibrium layer surrounding a dose point of interest. While Fano's theory applies to situations of charged particle equilibrium, the density scaling theorem by O'Connor (O'Connor, 1957) relates the dose in two media of different density but equal atomic composition, both irradiated by the same external beam, to each other. According to this theorem, the ratio of the secondary scattered photon fluence to that of primary photon fluence is constant in the two media provided all geometric distances, including field sizes are scaled inversely with density. This means that the dose at corresponding points in the two media is the same if all dimensions in the irradiation geometries are scaled inversely with density. Both Fano's and O'Connor's theorems rely on a common assumption that the interaction probability (per electron) is independent of density variations between media.

2.1.2 Kerma

The deposition of energy in tissue from a photon beam is fundamentally a two-step process; KERMA and absorbed dose:

1. The photons interact in the medium to impart kinetic energy to charged particles (e.g. the TERMA-total energy released in medium)
2. Charged particles then deposit their given energy through ionization and excitation events along a finite track (e.g. the dose step)

Kerma stands for the Kinetic Energy Released in the Medium

$$K = (dE_{tr} / dm)\left[\frac{energy}{mass}\right]$$

where dE_{tr} is the kinetic energy transferred from photons to electrons in a volume element of mass dm. It is the quantity that most directly connects the description of the radiation beam with its effects (Johns and Cunningham, 1983).

2.1.3 Absorbed dose

This is the quantity that is of more interest in radiotherapy and radiobiology. The absorbed dose is the energy actually retained in the medium and is brought about through the ionization and excitation events along the finite secondary particle tracks (Johns and Cunningham, 1983).

2.1.4 Primary and scattered dose components

One basic physical principle which has been used for many years in photon dose calculations involves partitioning the dose delivered to each volume element into two components – primary and scatter. The photons that enter through the surface of the patient or phantom are referred to as incident or primary photons. The first time such photons interact within the medium, they contribute to primary dose through secondary electrons. The scattered component is that part of the dose which is deposited by photons, which have previously interacted at least once in the medium. These two components obey the same physical laws (divergence, attenuation, generation of secondary photons and electrons), but have very different source distributions and energy spectra (Swinnen, 2005). Dose calculation models which achieve separation of these components have gained considerable success when calculating complex treatment plans.

2.2 Experimental quantities

To describe the penetration characteristics of photon beams, three quantities have been widely used: the percentage depth dose (PDD), the tissue phantom ratio (TPR) and the tissue maximum ratio (TMR). PDD data are impractical for direct reconstruction of dose distributions since they depend on the source to surface distance (SSD). Instead TPR's

being independent of SSD, have gained popularity. Another quantity, TMR has been used in some dosimetry systems (Khan, 2003). TMR is renormalized TPR data such that the specified reference depth is the depth of maximum dose. The uncertainties due to electron contamination of measurements at the depth of dose maximum is a complication, and use of a reference depth away from the build up region as in the TPR definition, is a better choice for dosimetry systems (Dutriex *et al*, 1997). Early dosimetric systems have tried to separate scatter from the primary dose using scatter factors to express the ratio of the total to primary dose at a point.

2.3 Treatment planning system

The functionality and quality of any RTPS is dependent on the type of algorithms used in the different steps of the planning process. Knowledge at some level of the various algorithms used within the RTPS can help the user understand the capabilities and limitations of the specific systems. Dose calculation models should serve, within the environment of a RTPS, to provide quick and accurate results for all relevant types of treatment field arrangements. RTPS require input data to their beam models for generating isodose curves and calculating monitor units. These data are generally obtained with a scanning water phantom system. The RTPS (Helax-TMS, 2003) at Johannesburg Hospital has two dose calculation algorithms available for external beam planning, the pencil beam (PB) and the collapsed cone (CC) algorithms. Dose calculations for patients on the Helax-TMS use electron density information from Computed Tomography (CT), based on the conversion from Hounsfield numbers (HN) , thus accounting for the attenuating properties of different tissues, as well as providing information on the material composition. Modern treatment planning techniques use highly advanced tools in order to conform the dose distribution to the target. The requirements for achieving accurate dose calculations have resulted in RTPS's utilizing calculations based on convolution techniques to achieve high accuracy as cited by Weber and Nilson (Weber and Nilsson, 2002). Any algorithm needs to take into account several different dose components, e.g. primary dose, dose from charged particle contamination, head scatter dose, and phantom scatter dose. For simplicity and speed in dose

calculations, models based on a PB kernel are frequently used for dose calculations. These kernels are generated by integrating Monte Carlo (MC) calculated point kernels (energy deposition in an infinite medium around a primary photon interaction point) over depth. The PB model has however been shown to have some limitations in heterogeneous media (Knoos *et al*, 1995). Lack of lateral scatter from heterogeneities, as well as disregard for the loss of electron equilibrium, may lead to specific errors in for example, the thoracic region. Other draw backs are due to the spatially invariant pencil kernel leading to an underestimation of the output for larger fields, whereas charged particle contamination models in some situations, lead to unwanted overestimations of dose in the build up region implying problems for in vivo dosimetry (Knoos *et al*, 1994). PB kernels have however, long found widespread application in electron beam dose calculation algorithms. The CC method is a specific approximation to the point kernel approach. The kernels are discretized in a number of directions, unevenly distributed in angle with a concentration in the forward direction where most of the photons are scattered (Ahnesjo, 1997). For each direction, the kernel h is analytically described by an exponential over r^2, r being the distance from the point of interaction, i.e.

$$h(r) = (Ae^{-ar} + Be^{-br}) / r^2$$

Where *A. a, B*, and *b* are fitting parameters depending on the scattering angle. The dose deposited during the ray trace is distributed into the patient volume according to the specification in the point kernels. All energy emitted in a solid angle cone is assumed to be transported along the cone axis, hence the name collapsed cone. The two algorithms differ primarily in how they model radiation transport and calculate dose in heterogeneous media, with the CC algorithm better approximating dose to the medium (Ahnesjo, 1989). It has been shown that there is little or no clinically significant difference in the calculation of dose by the two algorithms when no large non-unit density heterogeneities are present and under full scatter conditions, such as in the irradiation of the pelvis (Aspradakis, 2003). However treatment planning calculations of the chest wall are complex due to missing tissue, the thinness of the chest wall and the

presence of lung. The accuracy of calculated dose is in this case dependent on the type of algorithm employed (Aspradakis, 2006).

2.3.1 Monitor Unit (MU) Calculation

The calculation of the number of monitor units for the individual fields of a treatment plan is included in most modern RTPSs, however it is essential for the user of a RTPS to understand the principles of the MU calculation algorithm. Generally the MU calculation is closely linked to the calculation of the relative dose distribution. Due to the wide variation, both in monitor unit calculation algorithms and in clinical situations, it is difficult to indicate how much effort should be spent by each institution in testing algorithms for monitor unit calculations. Factors affecting these calculations and related quality assurance programmes have been discussed by Kutcher *et al*, as cited by Dutreix *et al* (Dutreix *et al,* 1997). Monitor unit calculations must also be compared with point/absolute dose (e.g. Gy) calculations as significant discrepancies of up to 5% have been observed (Starkschall *et al*, 2000). The proposed method for calculating MUs or dose (D) in a wedged asymmetric field, assuming an isocentric set-up (SAD = 100 cm) and treatment unit calibration k = 1 cGy/MU at the prescription point for a 10 cm x 10 cm reference field size at a source to calibration distance SCD = 100 + t_o (t_o is the maximum depth of maximum dose (Khan, 2003 and Mihailidis, 2000)) is given by

$$MU = D(\text{prescription})/q \quad \textit{where}$$

$$q = k * Sc(r_c) * Sp(r_d) * TMR(d, r_d) * (SCD / SAD)^2 * WF(d, r_d) * POAR_w(x, y, d) * Cf$$

where $Sc(r_c)$ is the collimator scatter factor for collimator field size r_c at central axis, $Sp(r_d)$ is the phantom scatter factor for equivalent size r_d at central axis, TMR (d, r_d) is the tissue-maximum ratio for the open field at central axis, WF (d, r_d) is the depth and field size dependent wedge factor at central axis, $POAR_w$ is the depth-dependent primary wedged off-axis ratio defined in open asymmetric fields. $POAR_w$ is the ratio of primary dose at the off-axis point of interest to the primary dose at the central axis at the same

depth, for a symmetrically wide open field (Khan, 2004). C*f* is the additional correction factor for attenuators such as block trays or compensators and the inverse square correction is performed from the calibration distance, *SCD*, to the treatment distance, $SAD = SSD + t_o$. The changes in the primary dose at a lateral distance from the central axis due to changes in the beam intensity are given by the factor $POAR_w$. However unlike open asymmetric fields, wedged asymmetric fields have a primary dose profile that is not created by the flattening filter alone. Thus, there is no radial symmetry of the $POAR_w$. $POAR_w$ is then a function of the off-axis distance and depth, $POAR_w(x, y, d)$.

2.4 Film dosimetry

Film dosimetry is based upon the calibration of the film response (Optical Density) at a specific depth in a phantom and then converting the film density to dose by using a calibration curve (Yeo *et al*, 1999). The mass energy absorption coefficient of typical x – ray films increases as the photon energy decreases. Softening of the photon spectra with depth in phantoms results in an over response as a function of depth (Burch *et al*, 1997). Radiographic films are a valuable tool in 2D dosimetry. Film offers several advantages such as high spatial resolution, 2D information with one single irradiation, a permanent record of the integrated planar dose distribution and suitability for use in inhomogeneous phantoms. Typical radiographic film consists of a radiation sensitive emulsion coated on a transparent polyester base. The emulsion consists of silver halide crystals (typically 95% silver bromide and 5% silver iodide suspended in gelatin as in the case of Kodak XV and XTL films). When the emulsion is exposed to ionizing radiation, ionization takes place in the silver halide film crystals that result in the formation of a latent image. The polyester film base is typically 0.2 mm thick and free from significant optical defects or impurities. The sensitive component, the emulsion, consists of gelatin and silver halide grains, which are typically 1 – 3 μm in dimension. There is a significant change that takes place in silver halide grains when the photographic emulsion is exposed to light, x rays or charged particles. Only adequately exposed grains will be developed and the remainder is left largely undeveloped, i.e. the small fraction that creates a low level darkening on the film referred to as “fog”. The theory of how this happens has not yet been fully

understood but Gurney and Mott have described a mechanism of latent image formation as shown in Figure 2.1 (Pai *et al*, 2007).

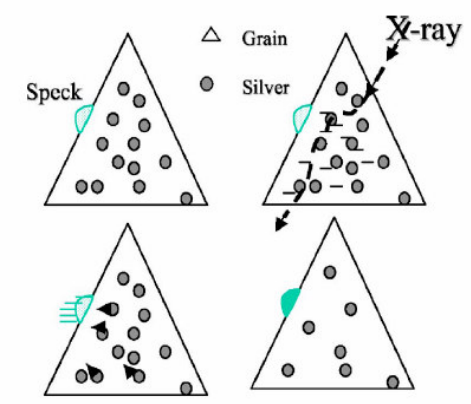


Figure 2.1 Gurney and Mott model of latent image. AgBr remains in the ionic form (Ag+Br−) in the crystal of the grain .Radiation produces ionization of Br− to Br_+e. These electrons make the speck negatively charged. The Ag+ migrate to neutralize the speck and forms a lump of Ag (aggregate) on the speck.

When the grain is ionized by radiation, the Br^- ions are split into Br and electrons:

$$\left(Br^- \rightarrow Br + e^-\right)$$

The electrons liberated migrate towards the specks, making the speck negatively charged, which in turn, attracts Ag^+ ions toward the speck, forming a latent image. Once the grains are developed, the grains comprising the latent image are converted to metallic silver, producing the dark regions on the film. Film developing includes four steps: developing, fixing, washing and drying. The value of film opaqueness is quantified through the light transmission factor (T) and is measured by a quantity called optical density (OD). The OD is a value describing the darkness of a film and is measured with a device known as a densitometer.

$$OD = -\log_{10}(T) = \log_{10}(I_o / I)$$

Where I_o is the incident light intensity measured in the absence of film and I is the intensity transmitted through the film perpendicular to the film plane. In dosimetry, the quantity of interest is the net optical density, defined as a measure of the difference between the unexposed processed film from the measured optical density. An extensive description of the relationship between optical density, grain size, and mechanism of photon interactions that relates to the optical density has been reported by Dainty and Shaw as cited by Pai *et al* (Pai *et al*, 2007). If α is the average area (cm^2/grain) of the developed silver grain and if there are n developed grains/cm^2 of film, then T can be written as

$$T = e^{-\alpha n}$$

$$OD = -\log_{10}(e^{-\alpha n}) = 0.4343\alpha n$$

It is difficult to know the number of electrons needed to develop a grain, but if we assume that a single electron is responsible for developing one grain, then one can correlate the electron fluence (ϕ) passing perpendicular to the film, to the optical density (Attix, 1986). If N is the number of silver bromide grains per unit area of the unexposed film, then n and OD can be written as:

$$n = \alpha N \phi$$

$$OD = 0.4343\alpha^2 N\phi$$

While the assumption is simplistic, it provides useful insights in OD film response. Because optical density is proportional to the number of silver grains per unit area and photon fluence, and because the photon or electron fluence is directly related to the radiation dose, the OD should be a function of dose. The relationship between dose and optical density is known as the sensitometric curve and is widely used in radiation dosimetry. Other characteristics of film can be plotted in various ways such as OD vs log (dose) known as the H & D curve (named after Hurter and Driffield). The H & D curve

provides the characteristics of the film in three sections: toe, gradient and shoulder. In diagnostic radiology, this type of graph shows the optical density range that provides the optimal diagnostic information. Sensitometric curves are used in film dosimetry for calibration purposes. The film linearity is important for dosimetry because film should be exposed to doses within the linear region (Hale *et al*, 1994).

The main challenges for using radiographic film as a megavoltage beam dosimeter is the dependence of OD on: (a) Photon energy, field size and depth in the phantom, (b) Film plane orientation with respect to the beam direction, (c)Emulsion differences amongst films of different batches, (d) Processing conditions (e)Method of densitometry and related artifacts (Pai *et al*, 2007).The implication being that the same optical density is not always associated with the same dose, making the conversion of OD to absolute dose difficult. In radiation oncology the dose versus OD presentation is used. The relationship between OD and dose depends strongly on the processing conditions, including developer temperature. OD increases as the developer temperature increases. Bogucki *et al* have shown that the optical density can be approximated as a function of temperature (Bogucki *et al*, 1997). Discrepancies in the magnitude of the effect of film orientation with respect to beam incidence have been reported. Burch *et al* observed no significant differences in optical densities due to film orientation (Burch *et al*, 1997) whilst on the other hand, Suchowerska *et al* showed that films exposed parallel to the beam axis had a measured over-response of about 15% at 25 cm depth in a phantom for a 10 cm x 10 cm field in a 6 MV or ^{60}Co beam (Suchowerska *et al*, 1999). Danclu *et al* found that the ratio of parallel to perpendicular response was almost unity except in the region around the dose maximum where the sensitivity for parallel response was about 4% lower for ^{60}Co, 6 MV and 15 MV photon beams (Danclu *et al*, 2001).

2.5 Thermoluminescent dosimetry

Thermoluminescent dosimeters (TLD) are used in radiation therapy for dose measurement in total body irradiation, brachytherapy, stray radiation and verification of dose delivery (Yu and Luxton, 1999). TLDs are used to confirm or determine radiation

dose to critical organs or to monitor special treatment. One of the commonly used TLD phosphors is TLD-100 (LiF), developed by the Harshaw Chemical Company. One merit of TLD dosimetry is that measurements can be carried out at different points placed inside solid phantoms simultaneously. With proper calibration, it is possible to obtain measured values with uncertainties within 3% (D'Angelo *et al*, 1999). The popularity of LiF-100 is due in part to its approximate tissue equivalence and low fading characteristics. A less desirable property however, is that it exhibits a non linear response with dose to certain types of radiation. The thermoluminescence (TL) output per unit dose is linear with dose up to 1 Gy, beyond which the response becomes supralinear (Folkard, 1989). TLDs of LiF in its purest form exhibit relatively little thermoluminescence, which is the phenomenon of photon emission subsequent to heating. The presence of impurities i.e., magnesium and titanium in TLD-100 LiF, appears to be necessary for radiation-induced TL. When a crystalline TLD is irradiated, a minute fraction of the absorbed energy is stored in the crystal lattice as shown in Figure 2.2.

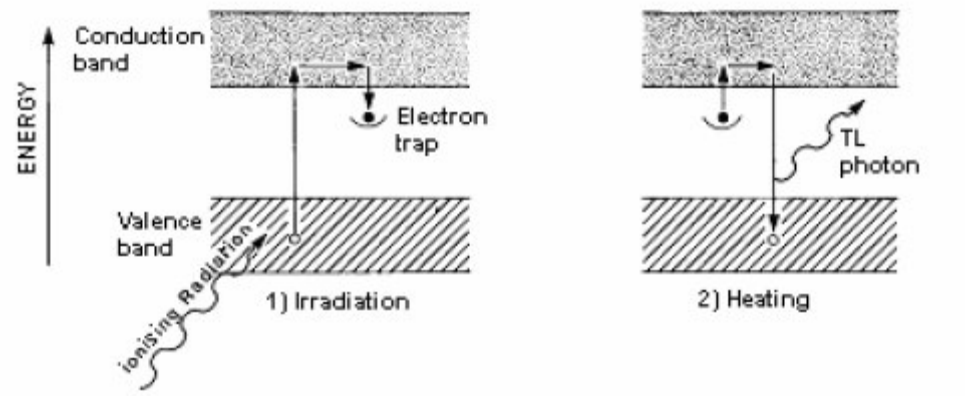


Figure 2.2 A simplified energy diagram to illustrate the thermoluminescence process (Khan, 2003).

The energy stored in the irradiated TLD is recovered as visible light by placing it on a planchet heater in a commercially available TLD reader and heating the TLD in a light tight chamber. A photo multiplier tube (PMT) placed in the TLD reader detects the light emitted from the TLDs. The arrangement for measuring the TL output is shown in Figure 2.3.

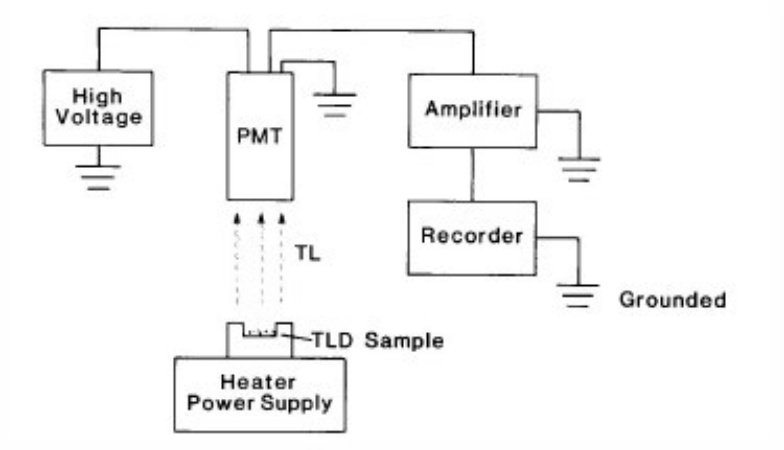


Figure 2.3 Diagram showing apparatus for measuring thermoluminescence (Khan, 2003).

The light output varies as the temperature is increased. The area under the glow curve, i.e. the total light output, is proportional to dose. Characteristics of TLD that are particularly important for radiation dosimetry include variability of the TL response with readout temperature, referred to as the glow curve. The variability of TL response relates to annealing procedures and the nonlinearity of the TL response. Zimmerman *et al* found that several prominent peaks in the TLD-100 glow curve decay at room temperature (Zimmerman *et al*, 1966). The peaks with longer half life are the most stable, and potentially the most suitable for radiation dosimetry. The peaks with shorter half life cause undesirable signals, which can be removed by various techniques of pre- and post-irradiation annealing. The presence of nitrogen gas in the planchet chamber has been observed to affect the precision of TLD reading, especially for radiation doses below 10 cGy. Meigooni *et al* found that for radiation doses below 5 cGy, there was a large standard deviation in TL response (almost 100% of the signal) when TLDs were read without nitrogen gas flow in the TLD reader, whereas the standard deviation dropped to 5% with nitrogen gas flow (Meigooni *et al*, 1995).

Unfortunately, TLDs have low reproducibility and high batch to batch variability. In order to achieve the highest accuracy, the 'most stable' TLDs must be selected and calibrated identically. The calibration includes irradiation and dose reading, followed by annealing which involves heating to a certain temperature (e.g. 400^{o}C) for an hour, cooling to room temperature and rechecking the sensitivity on the next day (Ertl *et al*,

1996). Using an array of TLDs inserted into a phantom can provide point dose information that can be reconstructed into a two dimensional dose distribution. The necessary corrections can be established by plotting the TLD reading against dose. A useful empirical formula to correct for the supralinearity is

$$C_{\text{supralin}} = \left(1 + 0.0278D - 0.000265D^2\right)^{-1}$$

Where D is the dose given (not the TLD reading) and C_{supralin} is the factor by which the reading must be multiplied in order to correct for supralinearity. This formula is satisifactory up to 20 Gy. The supralinearity correction is not altered as the chips age (Mayles, 1993). The angular dependence of TLD is only a problem in so far as the orientation of the chips can affect the size of the cavity. This is more important for electrons and brachytherapy where the dose gradient may be high. It is however sensible to irradiate normal to the flat face of the chips.

2.6 Computed Tomography

CT images are produced with a highly filtered, high-kV x-ray beam of average energy approximately 75 keV. Allan Cormack realized that it was possible to observe radiation transmission profiles of an object and use that data to compute an image of that object (Cormack, 1963). The transmission of x-rays through an object is given by

$$I = I_o e^{-\mu x}$$

Where I is the transmitted intensity, I_o is the initial intensity, x is the thickness of the uniform object, and μ is the linear attenuation coefficient. For non homogeneous media like the human body, the path along which the ray travels can be divided into a series of i elements (pixels) each with length (x_i) and attenuation coefficient (μ_i) such that the x-ray transmission through the series of elements is then given by

$$I = I_o e^{-(\mu_1 x_1 + \ldots\ldots \mu_n x_n)}$$

By moving the x-ray tube around the patient multiple transmissions can be obtained from different directions, resulting in many attenuation equations, which can be solved for μ_i. These attenuation coefficients then expressed as CT numbers,

$$CT\ numbers = 1000\left[(\mu_i - \mu_{water})/\mu_{water}\right]$$

Where μ_{water} is the linear attenuation coefficient for water. Water and air yield CT numbers of 0 and -1000 respectively. On an image, each CT number is assigned to a shade of grey for display and the entire matrix of CT numbers results in a cross sectional image of the object.

CT is used as an imaging device for diagnostic purposes. It provides a full (3-D) representation of the patient through a series of contiguous two dimensional (2-D) transaxial images. CT images consist of matrices of attenuation coefficients which are commonly used to construct a patient model in radiotherapy treatment planning. Part of the process is the conversion of CT numbers into electron density relative to water, for use in dose calculation. Routine measurement of CT number (and electron density) constancy is therefore a recommended part of the quality assurance programme in radiotherapy (Fraass *et al*, 1998). Accurate dose calculation not only requires accurate algorithm, but also accurate calibration of Hounsfield Unit (HU) for CT-based inhomogeneity corrections prior to dose calculation. Establishing a relationship between CT numbers and electron densities provides a simple method of correcting for inhomogeneous tissues. The possible errors in measured CT numbers need to be assessed in order to estimate the errors in calculated dose when the CT information is used directly (Papanikolaou *et al*, 2004). For instance, the CT number and thickness of bone cannot be measured accurately unless the thickness exceeds 3 mm. Below 3 mm there is a progressive underestimation of the CT number and an overestimation of thickness (Newman *et al*, 1998).

2.7 The radiotherapy procedure

Planning and delivering radiotherapy is a complex process which, for each individual patient, involves taking into consideration the definition of the target volume, decisions on total dosage, the fractionation schedule and the choice of appropriate radiation modality and method (Moller *et al*, 2003). There have been numerous steps in a radiotherapy process, which potentially causes a geometric discrepancy in patient/organ position between treatment planning and actual treatment delivery. In treatment simulation and planning, starting from patient positioning and ending at transferring the treatment plan to the radiotherapy machine, each step will introduce uncertainties in patient/organ geometry. On the other hand, most of the positioning steps will be repeated during the treatment delivery introducing the systematic and random variations in the patient/organ treatment geometry. The radiotherapy procedure includes: (a) Clinical investigation and type of treatment, (b) Radiotherapy Treatment Planning/ dose planning (c) Simulation (d) Irradiation (e) Follow up (f) Documentation and analysis

2.7.1 Beam combinations

Depending on the location of the tumor, several techniques and beam energies can be employed. The most common conventional techniques include a single beam, parallel opposed beams, a four field “box”, rotational techniques, coplanar and non coplanar beams.

2.7.2 Single photon beam

Single photon beams are of limited use in the treatment of deep seated tumors beyond the depth of dose maximum. Single fields are often used for palliative treatments or for relatively superficial lesions (depth < 5-10 cm, depending on the beam energy). For deeper lesions, a combination of two or more photons beams is usually required to concentrate the dose in the target volume and spare the tissues surrounding the target as much as possible.

2.7.3 Parallel opposed beams

Parallel opposed beams overcome the difficulty of a decreasing dose gradient due to each individual beam. A decrease in the depth dose of one beam is partially compensated by an increased contribution from the opposing beam resulting in a uniform distribution within the tumor volume.

2.7.4 Four field “box”

This is a technique of two opposing pairs of parallel opposed beams at right angles to each other, producing a relatively high dose “box” shaped region. The region of highest dose occurs in the central portion of the volume that is irradiated by all four fields. This technique is commonly used for treatment of central organs in the pelvis.

2.7.5 Treatment verification

Treatment delivery encompasses a multi-faceted process to ensure that treatment delivery is implemented in accordance with the planned intention. Quality control helps to ensure that radiotherapy is administered safely and accurately and facilitates assessment of the reproducibility of treatment setups. Following localization and planning procedures, a simulator may be utilized to verify the treatment plan prior to its implementation on a treatment unit (e.g. verifying planned treatment fields, gantry angles, etc). This will confirm the appropriate coverage or avoidance of normal tissue structures. Various methods, materials and devices are conventionally used to try and reproduce patient position. These include sagittal and lateral lasers together with patient anatomical references e.g. supra sternal notch. Other aids may include immobilization devices such as breast boards, head and neck immobilization devices, etc. Installation and use of computerized record and verify systems (CRVS) help prevent treatment errors prior to treatment delivery. Data entered in the system before treatment delivery is available as a reference throughout the treatment course. CRVS verify a wide range of treatment

parameters, including: (a) Patient name and identity number verification, (b) Mode of treatment, (c) Treatment field, (d) Cumulative doses, (e) Fraction number.

Dose verification is as crucial as verifying the field placement position as it is the most obvious method of assessing the accuracy of patient's treatment. Radiation detectors such as TLDs, semiconductor devices like silicon diodes and portal films are routinely employed in verification dosimetry (Cherry and Duxbury, 1998). Cylindrical phantoms of the appropriate radii are useful for simulating body and limb cross sections. However these homogeneous phantoms with regular shapes are not a good representation of a real patient and can give a misleading impression of the accuracy of computer calculations. The anthropomorphic phantom used in this work is affordable as compared to the commercially available humanoid phantoms. In certain clinical situations, in-vivo measurements can give unexpected results, even when the uncertainties in the measurements have been accounted for. Treatment planning algorithms should be verified by designing appropriate phantoms to test potential weaknesses. In-vivo measurements can be made but, because they introduce additional uncertainties, surface doses are not a useful test of dose calculation algorithms. This work presents a method of assessing the dose directly in a patient-like phantom as clinically this is restricted to placing TLDs on the surface of a patient.

3.0 METHODOLOGY

3.1 Phantom fabrication

The pelvic anthropomorphic phantom that was used was fabricated at the Pretoria Academic Hospital, Department of Radiation Oncology (Kanduza, 2005). Perspex was used for the soft tissue, wax for the tumor volume and rectum, and plaster of paris for the left and right femurs of the pelvis based on mass attenuation coefficients, electron density and effective atomic number. External and internal contours of organs were fabricated based on the anthropomorphic phantom dimensions (Kanduza, 2005). The central part of the phantom accommodated circular inserts shown in Figures 3.1 and 3.2. Insert 1 was designed as the diagnostic anatomical insert and insert 2, the dosimetric verification insert. Insert 1 was used only for field design and placement. Insert 2 was designed to accommodate both TLDs and therapy verification film. These inserts were easy to exchange and could be repositioned in the phantom precisely. Figure 3.3 shows the position of film relative to the TLD positions in insert 2.

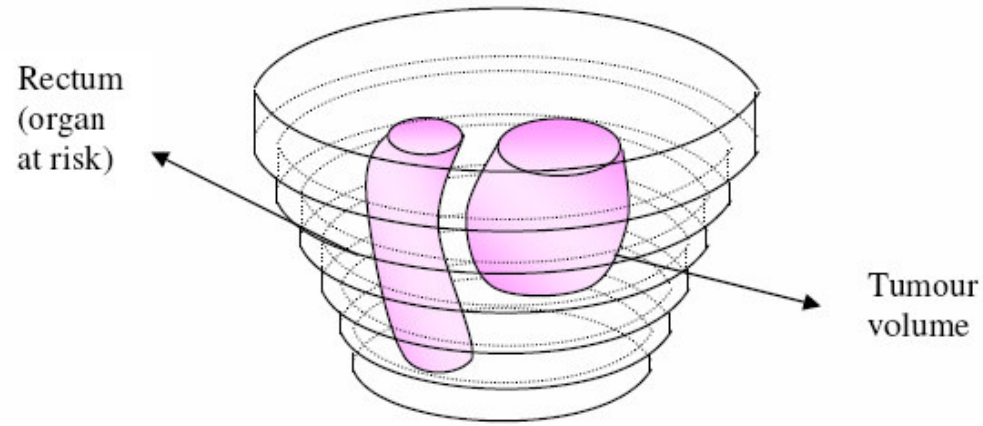


Figure 3.1 Diagnostic Imaging insert 1 (Kanduza, 2005).

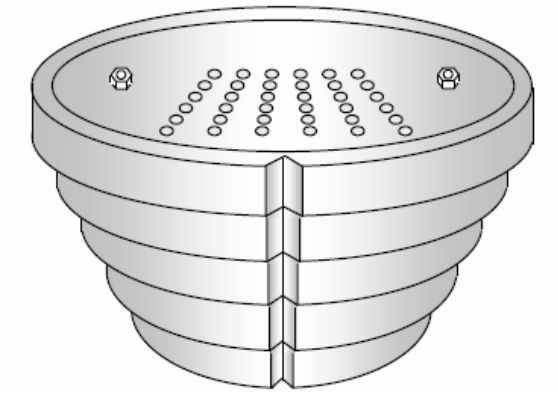


Figure 3.2 Dosimetric insert 2 (Kanduza, 2005).

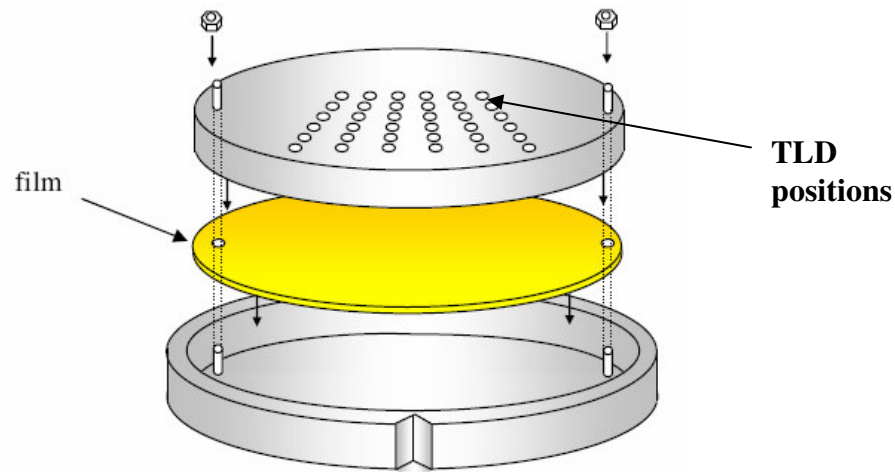


Figure 3.3 Positions of film and TLDs in the Dosimetric insert (Kanduza, 2005).

3.2 TLD Procedure

The Harshaw TLD System (Model 3500 Manual TLD Reader) was used for calibrating and reading the exposed TLDs. The Element Correction Coefficient (ECC) was used to compensate for the variations in sensitivity between dosimeters. This factor is a dimensionless parameter and it served to correct the sensitivity of each dosimeter in a batch to the average sensitivity of the batch. The TLDs were placed in a diagonal fashion, at dose points from the top left TLD position to bottom right and at the two opposite corners i.e bottom left and top right positions of the mid-axial insert. The same dose points were repeated throughout this experiment. Not all the TLD positions were used during the irradiations, which resulted in small air gaps.

3.3 Calibration and irradiation process

Lithium fluoride thermoluminescence dosimetry chips were used (TLD_100, Harshaw). A total of 40 TLDs were prepared for this work. All TLDs were handled with vacuum tweezers (to avoid scratches and contamination) and kept in dedicated trays. The radiation sources were 6 MV and 15 MV x-ray beam from a Siemens Primus M medical linear accelerator (Linac). The linac was calibrated isocentrically according to the TRS 398 dosimetry protocol (IAEA TRS 398, 2001) to an isocentric output of 1.00 cGy/MU at the depth of maximum dose, in a water phantom, in the reference field size of 10 x 10 cm^2. A Poly-Methyl-Methacrylate (PMMA) phantom was used to irradiate a batch of TLDs at 5 cm water-equivalent depth. After exposure to 1 Gy, the TLDs were read to generate their respective ECCs. The TLD software was set to reject TLDs that had sensitivities of more than ±20% of the mean response. All 40 TLDs met this selection criterion. After readout, all TLDs were kept in a tray with identification for sorting purposes. A reader calibration factor (RCF) within the TLD reader software was used to convert the measured signal into dosimetric units.

Direct measurement for treatment verification was therefore given by:

$$Dose(Gy) = reader\ output\ (reader\ units) * RCF(Gy / reader\ unit) * ECC$$

The percent deviation of all measurements was defined as:

$$\%Dev = \left[\left({}^{calculated\ dose}\!/_{Measured\ dose} \right) - 1 \right] * 100$$

where the calculated dose was derived from the planning system and the measured dose was the dose obtained from the phantom under radiation.

For the phantom irradiations, 35 TLDs were placed in insert 2 at the points of interest, inserted into the Anthropomorphic phantom and exposed to 70 cGy delivered using either the AP/PA or the four field "box" technique at 6 MV or 15 MV photon beam energy. Four TLDs were used as controls to monitor the TLD sensitivity following each annealing cycle. These TLDs were selected randomly from the batch of 40 TLDs and exposed to known doses of 0.5 Gy, 0.7 Gy, 1.0 Gy and 1.5 Gy before irradiation of the phantom. One TLD was not used. The variation of TLD output throughout the experiment was plotted as a function of the dose as shown in Figures 3.4 and 3.5 at 6 MV and 15 MV respectively. This provided a means of monitoring the sensitivity of the entire batch of TLDs after each annealing cycle and assessing the overall uncertainty. A typical cancer of the cervix protocol (used at Johannesburg Hospital) and a similar protocol using a 7 cm x 7 cm field size were used to develop the treatment plans (AP/PA and four field box).

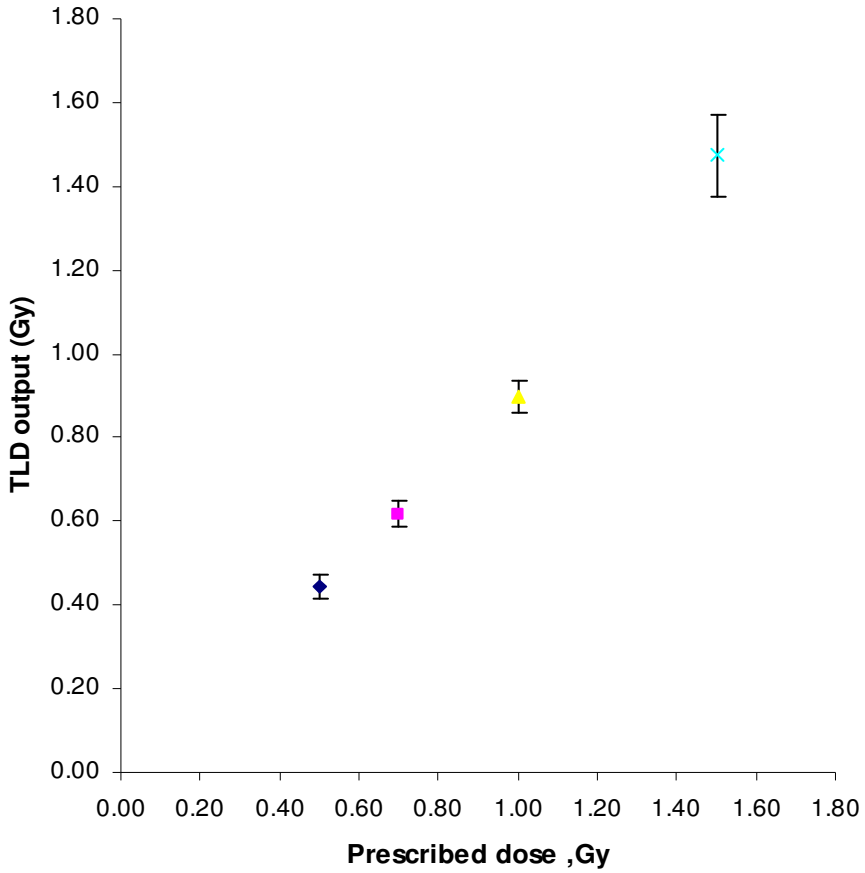


Figure 3.4 Variation of TLD output (Gy) with dose (Gy) at 6 MV. The error bars represent the overall deviations in the measurements.

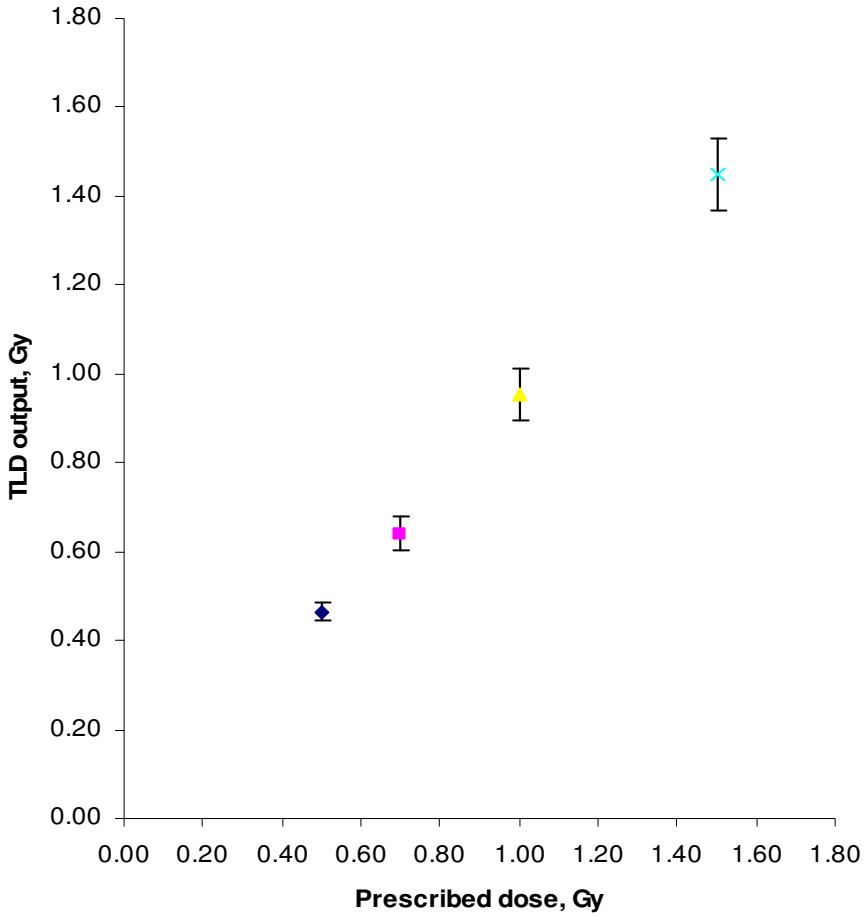


Figure 3.5 Variation of TLD output (Gy) with dose (Gy) at 15 MV. The error bars represent the overall deviation in the measurements.

3.4 Film calibration

The densitometer used had a calibration certificate traceable to the National Institute of Standards and Technology (NIST). Before use, the densitometer was calibrated using the calibration film that was provided with the densitometer. All films were irradiated, processed and measured at the Johannesburg Hospital Radiation Oncology Division for calibration purposes, the film was placed at the isocenter sandwiched in between PMMA sheets using the perpendicular geometry. The set up was similar to that used for calibrating the TLDs. For each of the photon beams, the films were irradiated to different

doses covering the range from 0.1 Gy to 0.8 Gy and a sensitometric curve produced as shown in Figure 3.6.

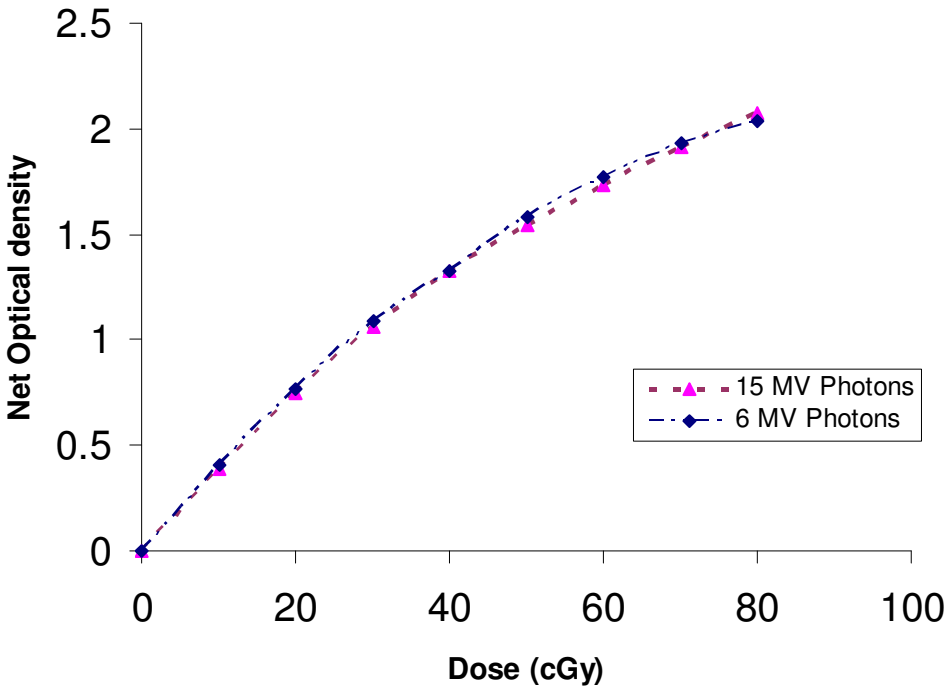


Figure 3.6 Sensitometric curves at 6 MV and 15 MV for the perpendicular setup. The uncertainties were very small and hence error bars are not visible.

The films were irradiated over a single day, and at the end of the irradiation period, all films including one which was not irradiated, were processed under the same conditions using an automatic film processor operating at 34^{o}C. The time between film exposure and processing was approximately 1 hour. It has been shown that a decrease in optical density of about 3% (for a dose of 0.45 Gy) and 1.8% (for a dose of 1.5 Gy) would be observed per month of delay between film irradiation and processing (Novotny *et al*, 1997). The film was used to obtain the 2D dose distributions. The films were exposed in their envelopes. For the films to fit into the phantom inserts, the envelopes were cut and made light tight using black insulation tape. A light proof test was conducted. The nuts on the phantom rods were then tightened to compress the film and to expel as much air as

possible from the film envelopes. The isodoses recorded on film were generated at the Pretoria Academic Hospital using the Vidar RIT Dosimetry Pro film scanning system.

3.5 Dose calculation on Helax-TMS

The phantom was immobilized in a polyurethane, air equivalent cast and CT scanned in order to generate three dimensional images and to avoid treatment position uncertainties. Reference markers were used to enable repositioning during treatment delivery. A CT scan incorporating these markers was acquired with a 0.5 cm slice separation and this data set was transferred to Helax-TMS RTPS. The external contour (skin) and organs at risk were outlined. The phantom was then planned with 6 MV and 15 MV beams using the standard local technique for cancer of the cervix and a smaller field size of 7 cm x 7 cm in terms of the isocentric placement and field borders. Dose calculations were carried out with both the PB and CC algorithms, both with and without inhomogeneity correction using the local cancer of the cervix protocol. The option of no inhomogeneity correction simply assigned all tissues in the patient geometry to unit mass density. This was done in order to compare the influence of tissue density on the dose calculations and to enable comparison to a manual 2D system of dose calculation. The isocentric planning technique was employed in this study. The plan normalization/prescription point was set to the isocenter. The treatment protocols obtained from the planning system are shown in Table 3.1. The dose distributions in the central plane normalized to 100% at the isocentre are shown in Figures 3.7 to 3.16. The PB algorithm was used to obtain point doses because in this mode it was possible to obtain point doses at TLD positions which was not possible with the CC algorithm.

Table 3.1 Treatment protocol showing the number of MUs needed to deliver 0.7 Gy to the isocenter for no inhomogeneity, manual calculation PB algorithm and CC algorithm.

Technique	4 Field Box				AP /PA	
Beam Number	1	2	3	4	1	2
Beam Label	Ant	Right	Post	Left	Ant	Post
Beam Quality	15/6	15/6	15/6	15/6	15/6	15/6
Radiation Type	Photons	Photons	Photons	Photons	Photons	Photons
Gantry angle	0	270	180	90	0	180
Treatment technique	Iso	Iso	Iso	Iso	Iso	Iso
SSD (cm)	90.3	81.9	90.7	82.3	90.3	90.7
Collimator Type	Symmetric	Asymmetric	Symmetric	Asymmetric	Symmetric	Symmetric
Beam Width [x] cm	16	12	16	12	16	16
Beam Length [y] cm	16	16	16	16	16	16
No Inhomogeneities MUs to deliver 0.7 Gy to the isocenter (15MV/6 MV)	24.8/28.4	16.5/18.9	24.8/28.4	16.5/18.9	37.5/41.3	37.5/41.3
PB MU's to deliver 0.7Gy to the isocenter (15MV/6 MV)	24.8/28.4	16.5/18.9	24.8/28.4	16.5/18.9	37.5/41.3	37.5/41.3
CC MU's to deliver 0.7 Gy to the isocenter (15MV/6 MV)	25.2/28.7	16.8/19.1	25.2/29.7	16.8/19.1	37.9/41.8	37.9/41.8
Manual MU calculations to deliver 0.7 Gy to the isocenter (15MV/6MV)	24.8/28.4	16.5/18.9	24.8/28.4	16.5/18.9	37.5/41.3	37.5/41.3

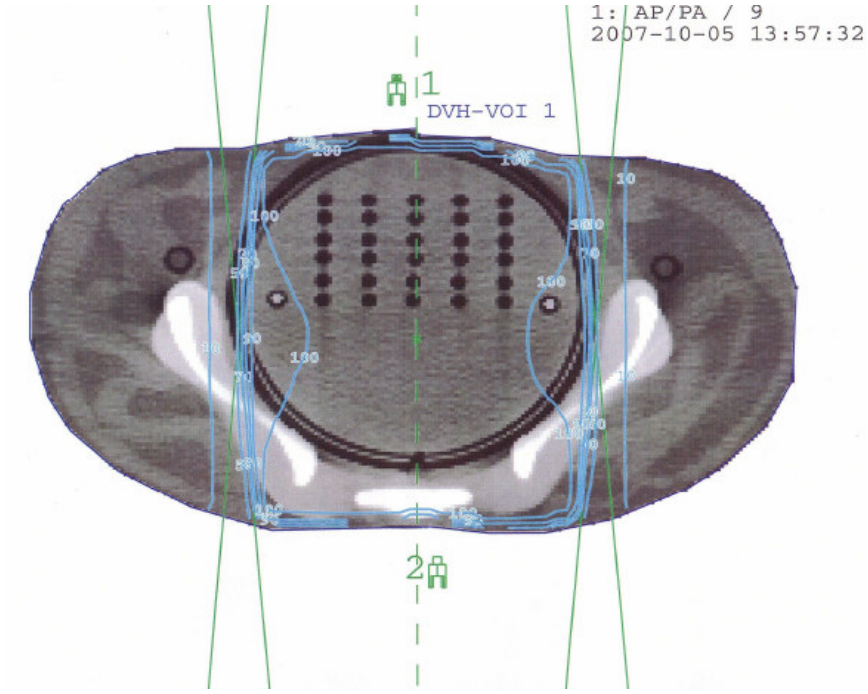


Figure 3.7 Pencil Beam parallel opposed axial dose distribution at the level of the isocenter using 6 MV beams.

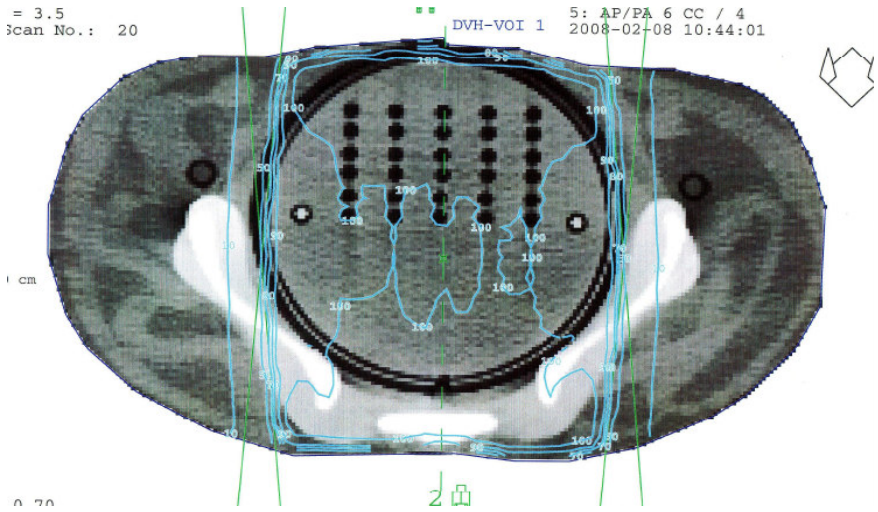


Figure 3.8 Collapsed Cone parallel opposed axial dose distribution at the level of the isocenter using 6 MV beams.

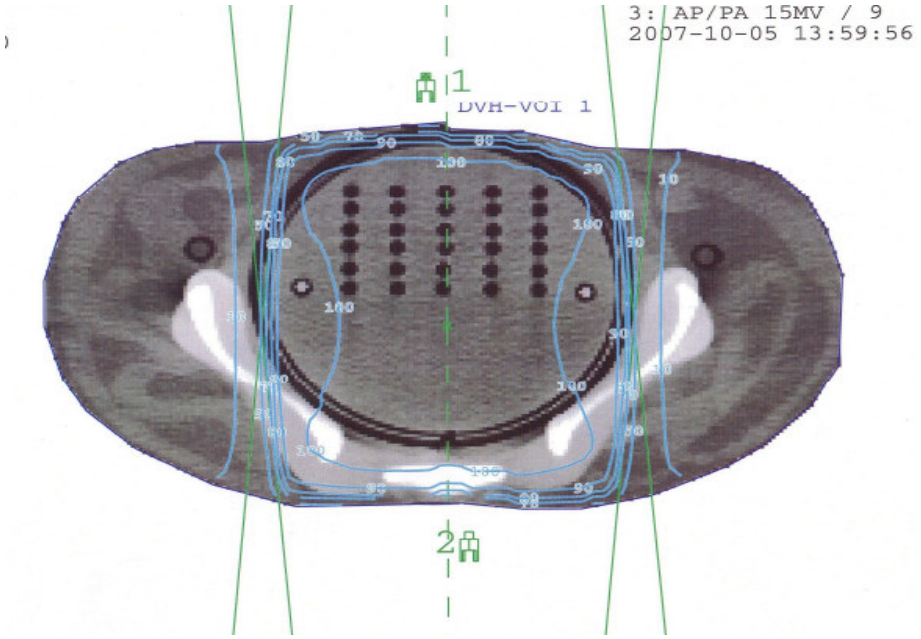


Figure 3.9 Pencil Beam parallel opposed axial dose distribution at the level of the isocenter using 15 MV beams.

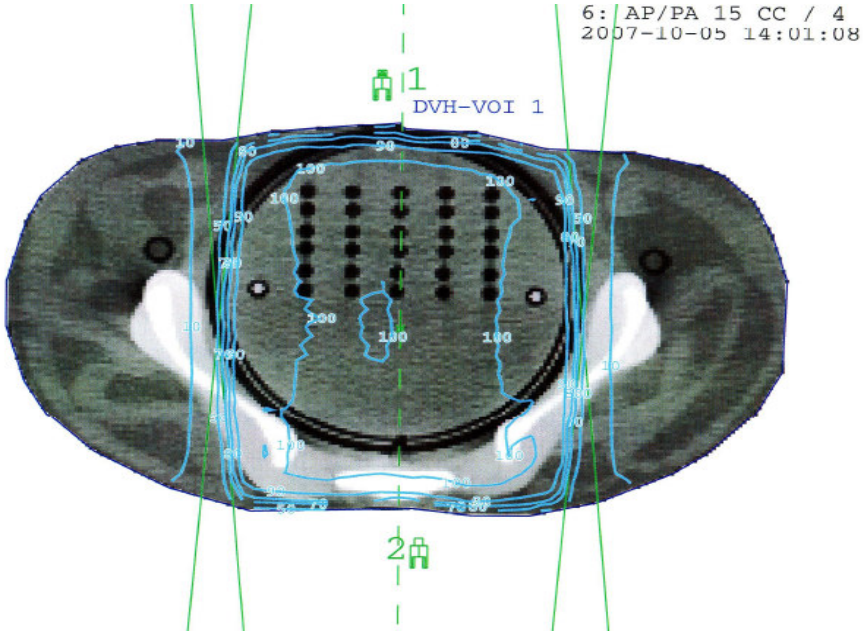


Figure 3.10 Collapsed Cone parallel opposed axial dose distribution at the level of the isocenter using 15 MV beams.

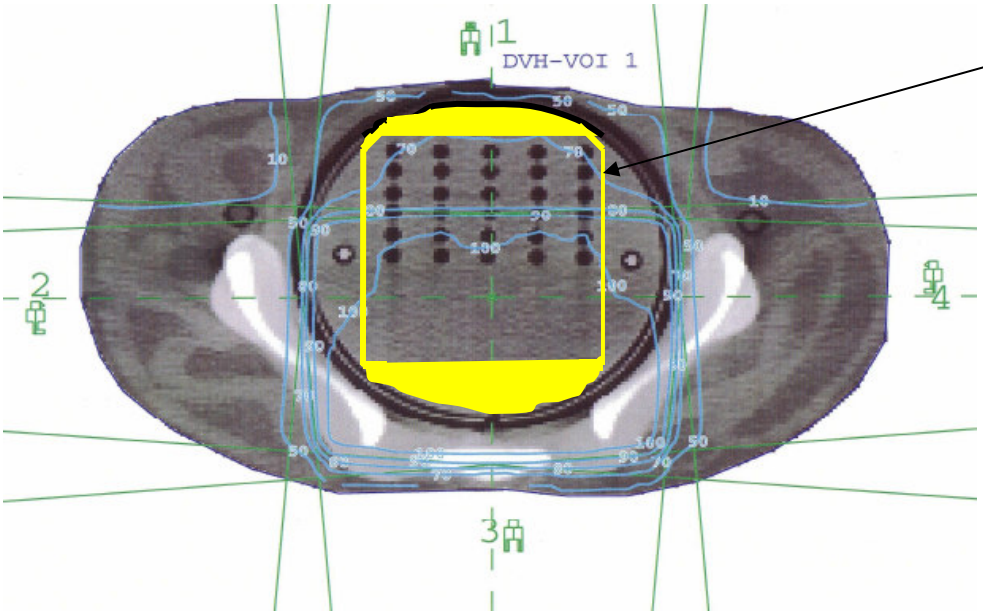


Figure 3.11 Pencil Beam four field "box" axial dose distribution at the level of the isocenter and the position of the cut film using 6 MV beams.

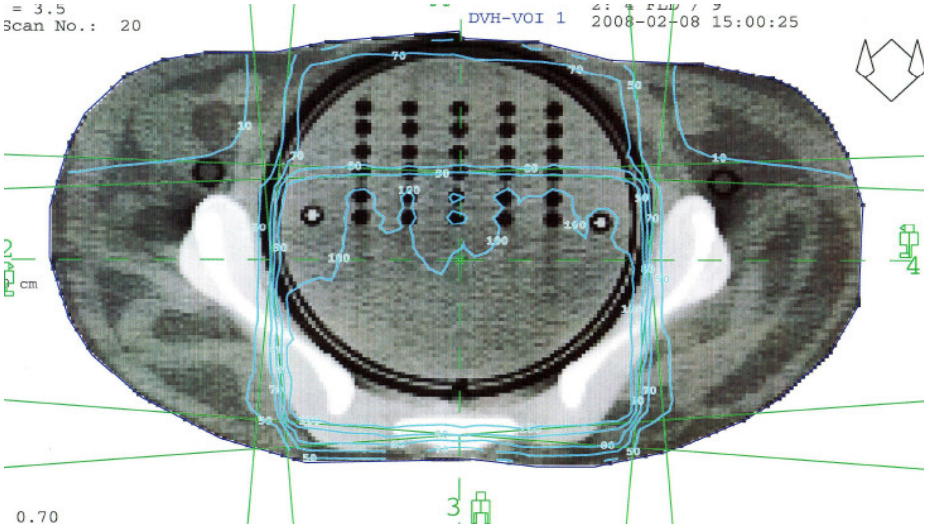


Figure 3.12 Collapsed Cone four field "box" axial dose distribution at the level of the isocenter using 6 MV beams.

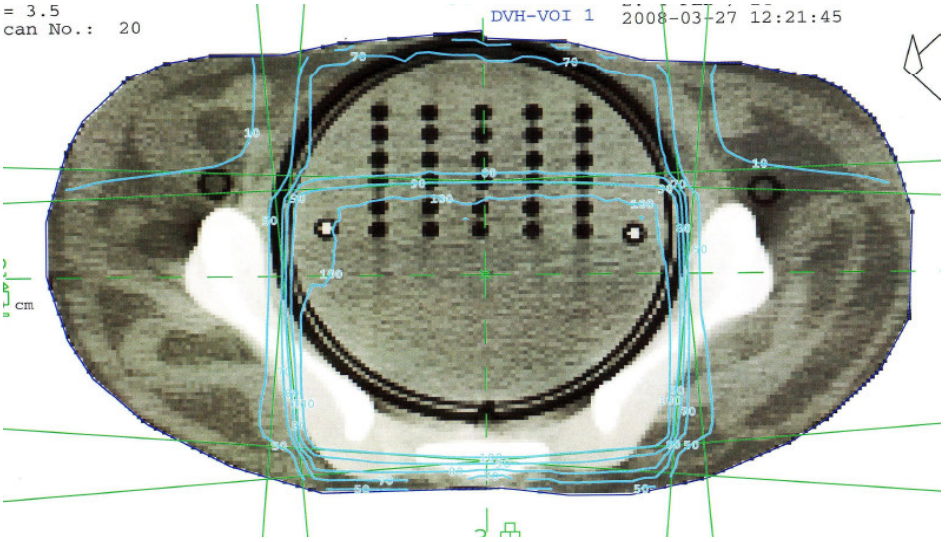


Figure 3.13 Pencil Beam four field "box" axial dose distributions at the level of the isocenter using 6 MV beams.

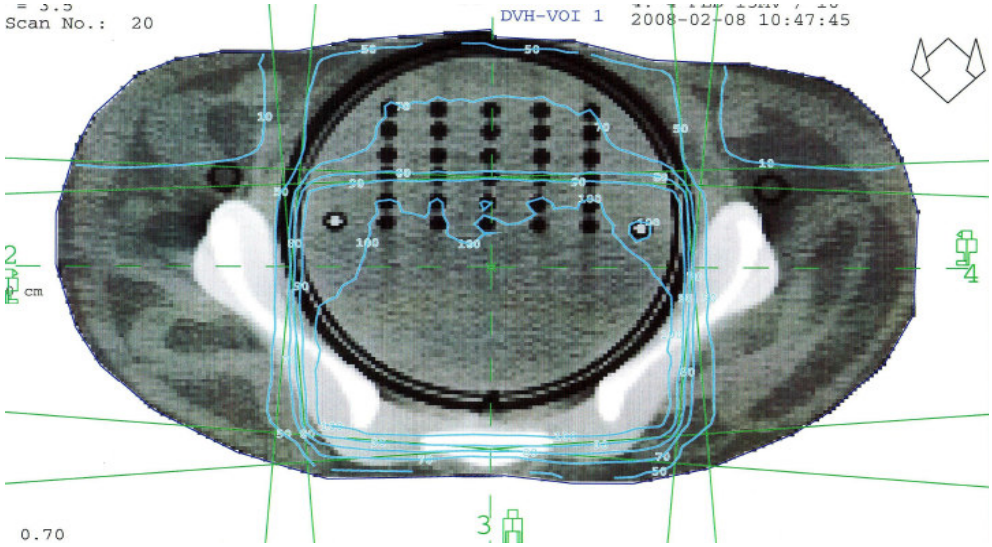


Figure 3.14 Collapsed Cone four field "box" axial dose distributions at the level of the isocenter using 15 MV beams.

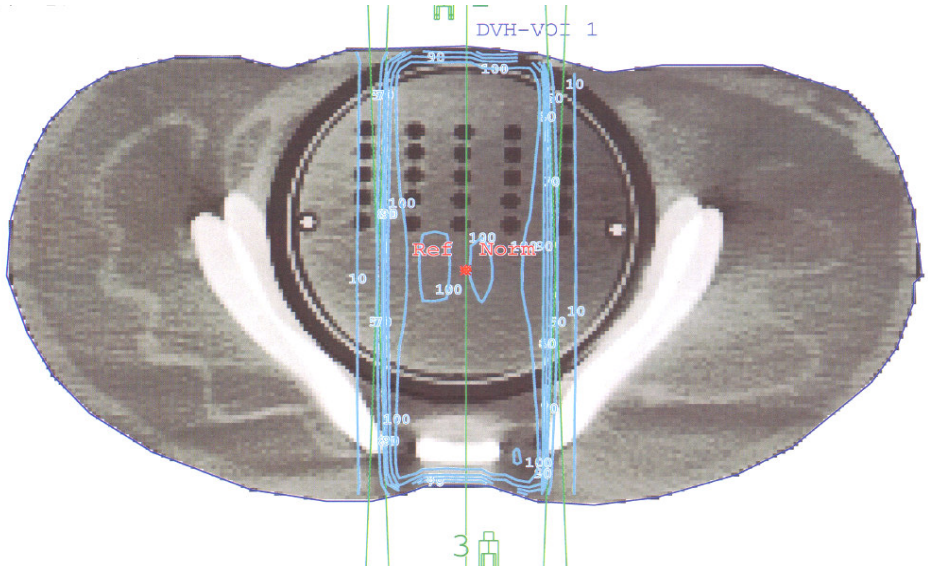


Figure 3.15 Pencil Beam parallel opposed axial dose distributions of a 7 cm x 7 cm field at the level of the isocenter using 6 MV beams.

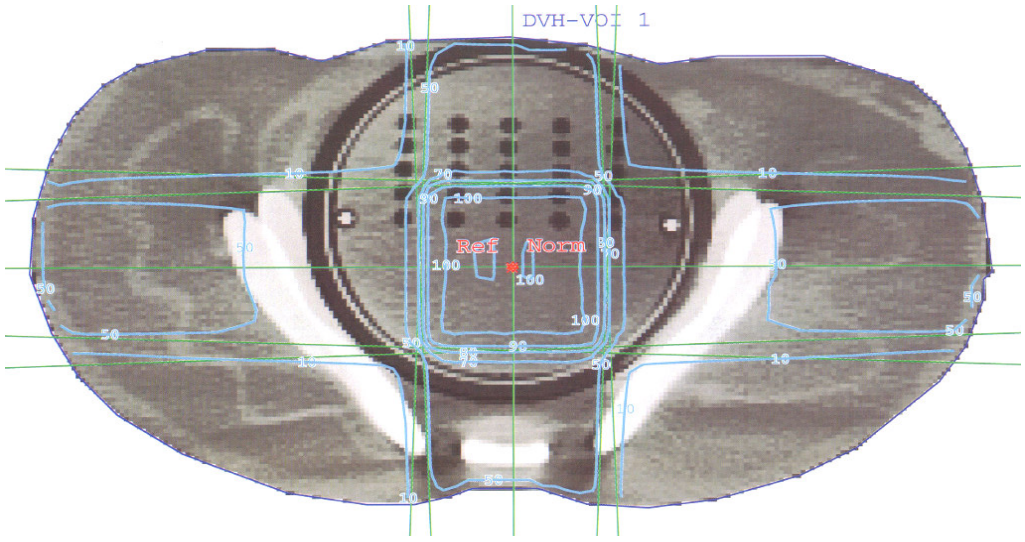


Figure 3.16 Pencil Beam four field “box” axial dose distributions (7 cm x 7 cm box) at the level of the isocenter using 6 MV beams.

4.0 RESULTS

The TLD results are given in appendix A. They show results of both the local cancer of the cervix protocol and when a smaller field size of 7 cm x 7 cm was employed. Figures 4.1 to 4.4 show the comparison between the doses measured by the TLDs using the AP/PA and the four field "box" technique to the doses calculated by the planning system at both 6 MV and 15 MV. On average, the measured doses were lower than those calculated by the planning system as is indicated by the line of agreement. Figures 4.2 and 4.4 show the different dose gradients that emerged from using the 4 field technique indicating regions of low, intermediate and high dose gradient.

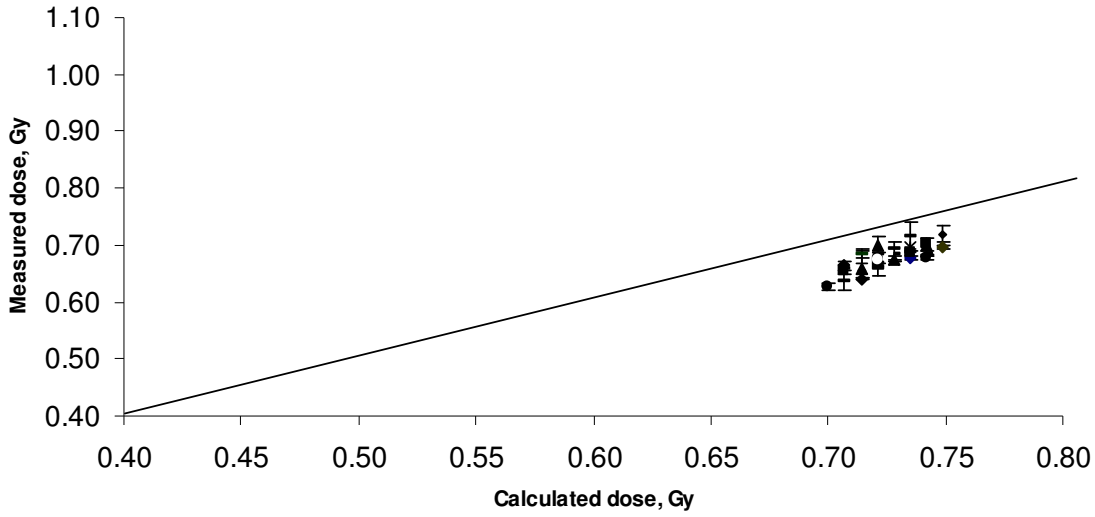


Figure 4.1 The comparison between the dose measured by the TLD's using the AP/PA technique to the dose calculated by the PB algorithm at 6MV.

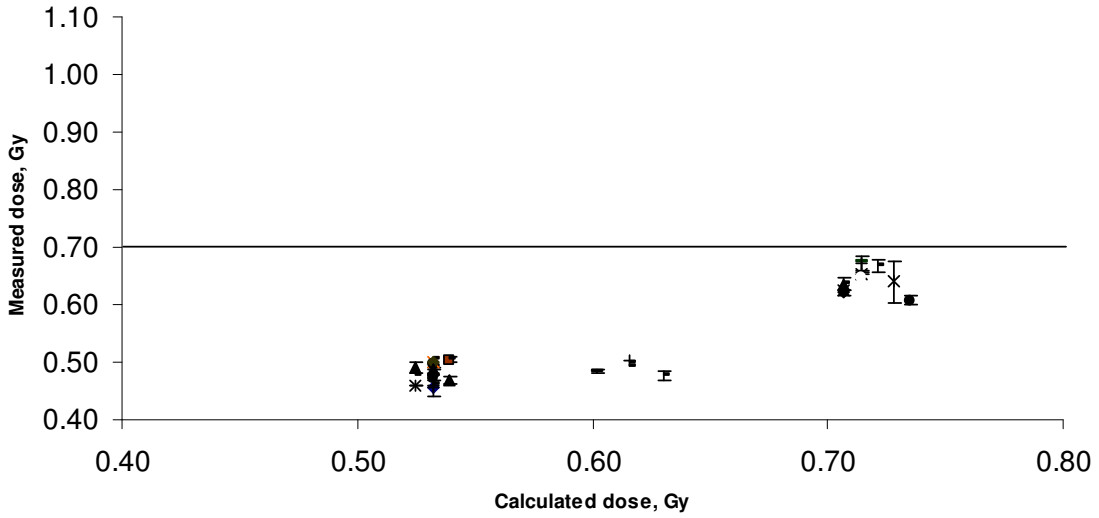


Figure 4.2 A comparison between the dose measured by the TLD's and the dose calculated by the PB algorithm using the four field "box" technique at 6MV. Three dose regions dose emerged, those of low, intermediate and high dose gradient.

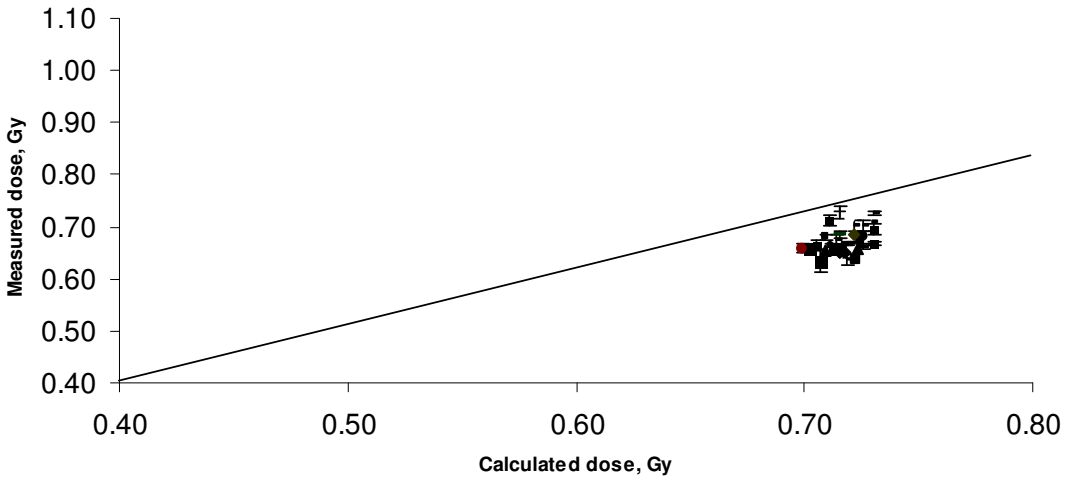


Figure 4.3 A comparison of measured dose with that calculated by the planning system for the AP/PA technique at 15 MV using TLDs. The PB algorithm was used to calculate the doses.

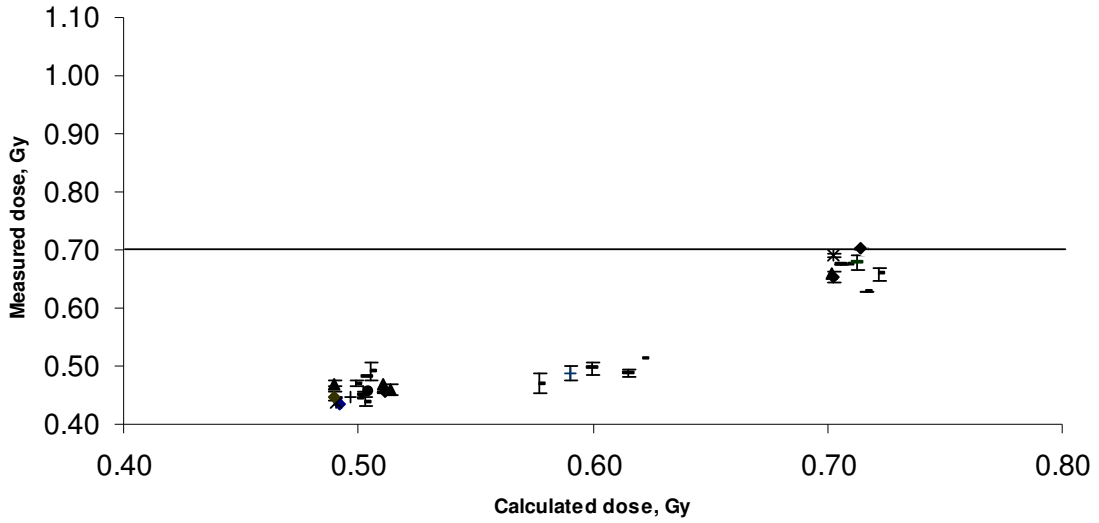


Figure 4.4 A comparison between the dose measured by the TLD's and the dose calculated by the PB algorithm using the four field "box" technique at 15MV. Three dose regions emerged, those of low, intermediate and high dose gradient.

The ratios of the dose measured by the TLDs to the calculated dose (when the local cancer of the cervix protocol was followed) are shown in Figures 4.5 - 4.8. The mean value of the difference between the calculated and measured doses for the AP/PA at 6 MV and 15 MV was 0.94±0.02 and that of the four field technique at 6 MV and 15 MV was 0.91±0.05. Three dose regions emerged for the four field technique*, those of* low, intermediate and high dose gradient, figure 4.*2* and 4.4. The four field technique for 6 MV gave a dose deviation from -4.9% to -32.1% and at 15 MV from -1.5% to -20.6%. For 6 MV and 15 MV parallel opposed beams, percentage dose deviations from -2.7% to -11.8% and from +0.2% to -11.5% were observed respectively. Tables A.1 to A.6 in the appendix give the individual TLD results for the techniques used in this study and also show the difference between the calculated and measured doses at 6 MV and 15 MV. Tables A.5 and A.6 also show optical density results measured at TLD positions and their corresponding doses when a smaller field size (7 cm x 7 cm) is used. Both the TLD and film dosimetry results obtained were lower than that predicted by the planning system. The results for the local cancer of the cervix protocol and a 7 cm x 7 cm field size placement are shown in appendix A, figures A1 and A2. The results for film (OD) when a

local protocol was followed were not included in the results. Film was over exposed due to the large field size resulting in high OD values and dose points that could not give any meaningful OD readings.

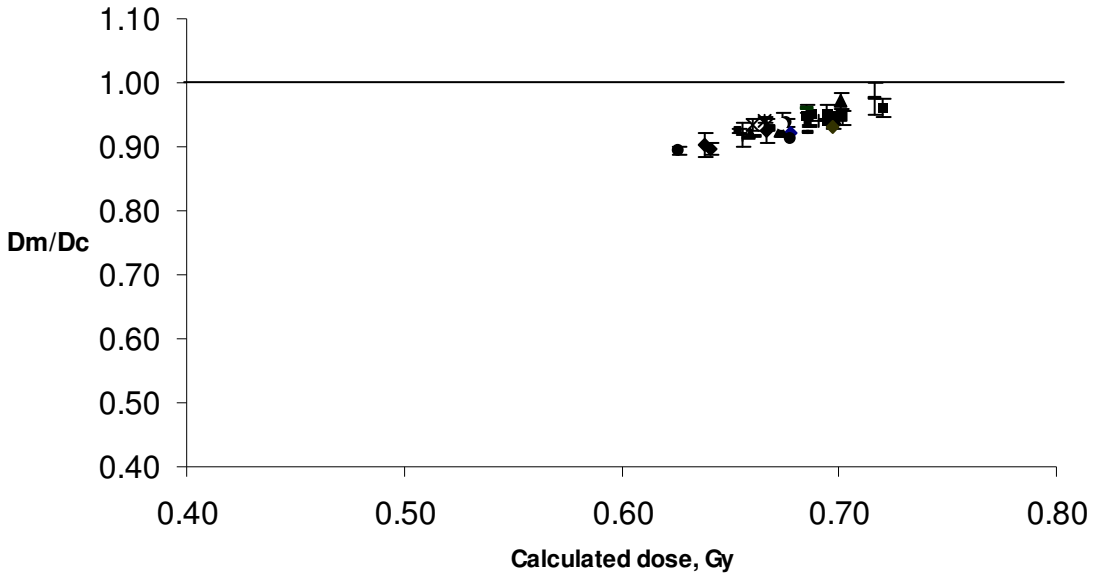


Figure 4.5 Ratio of measured to the calculated doses vs calculated doses for the AP/PA at 6 MV using TLDs. The PB algorithm was used to calculate the doses.

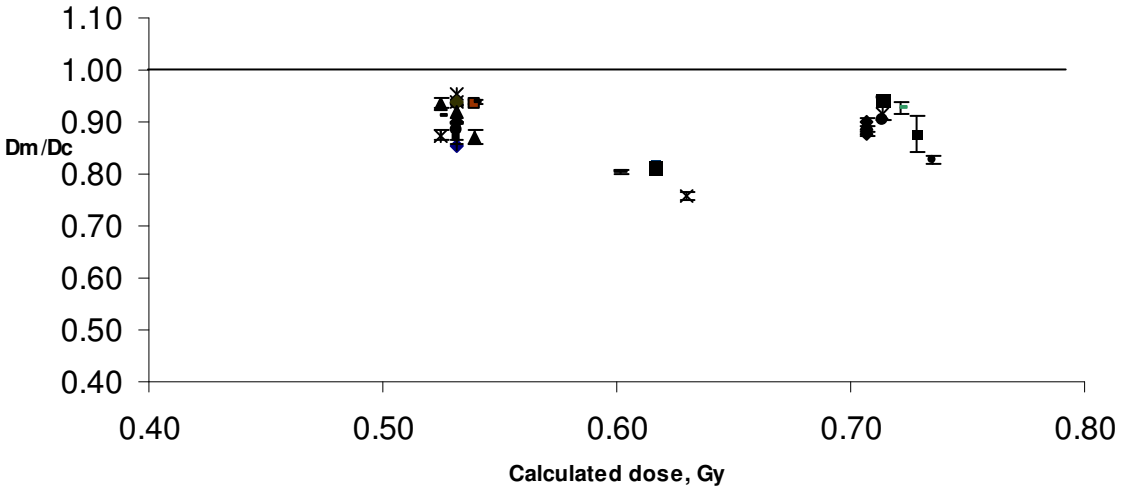


Figure 4.6 Ratio of measured to the calculated doses vs calculated doses for four field “box” at 6 MV using TLDs. The PB algorithm was used to calculate doses.

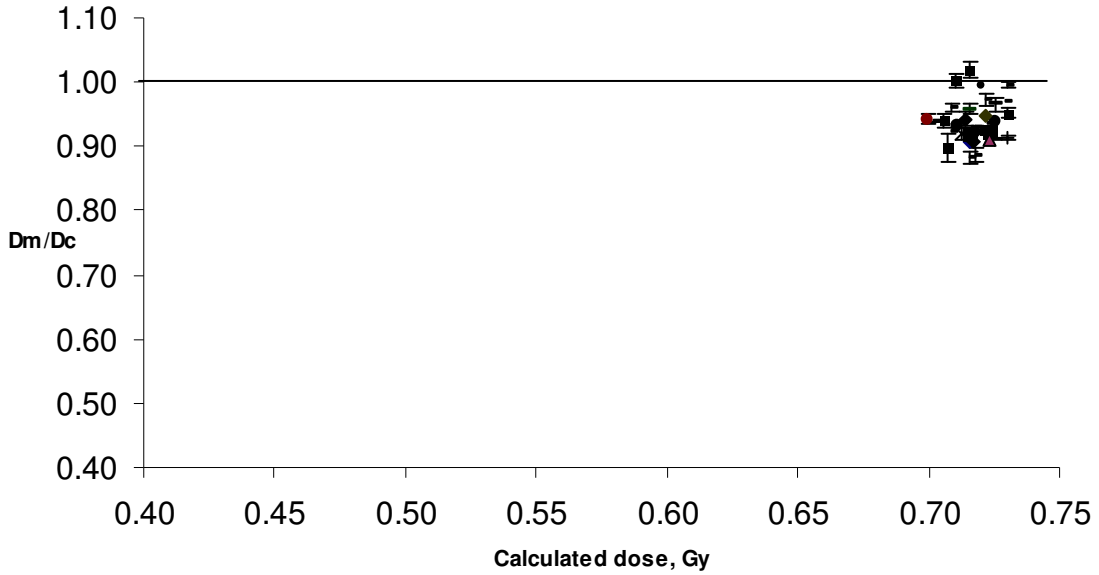


Figure 4.7 Ratio of measured to the calculated doses vs calculated doses for AP/PA at 15 MV using TLDs. The PB algorithm was used to calculate doses.

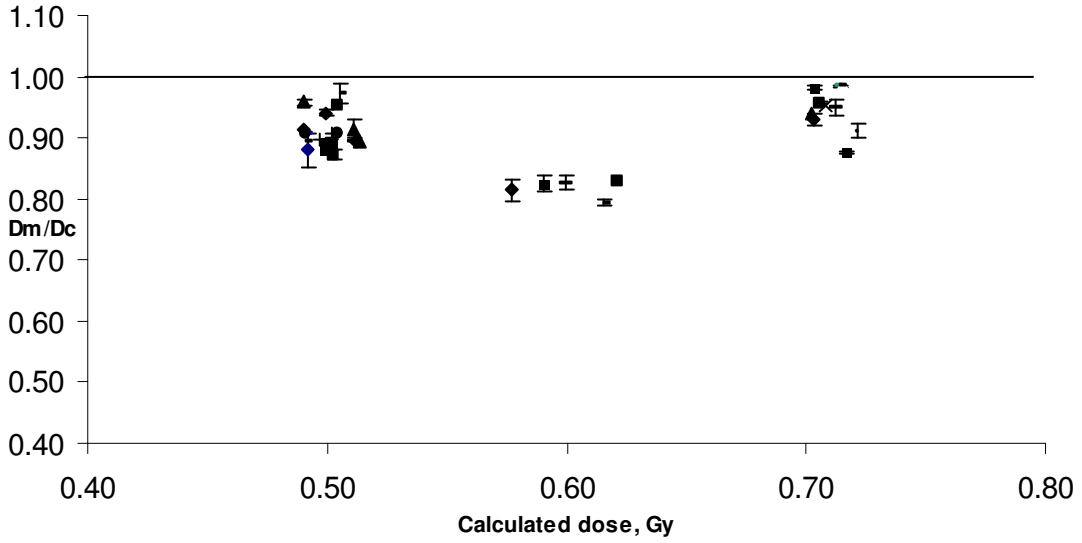


Figure 4.8 Ratio of measured to the calculated doses vs calculated doses for four field "box" at 15 MV using TLDs. The PB Algorithm was used to calculate point doses

5.0 DISCUSSION

The treatment planning process consists of various steps, including the calculation of the relative isodose distribution and the treatment time for each individual field. A manual check of a complex dose distribution in inhomogeneous volumes is usually not considered to have the same accuracy as a RTPS calculation, since computer algorithms are sophisticated and able to handle the physics of the radiation interactions more accurately. Nisbet *et al* observed that for the same input data set, the CC algorithm with Helax-TMS version 6.1 improved the agreement between calculated and measured dose in the build up compared with version 5.1A, where significant discrepancies were present. The reason for the differences between the versions was not stated and this confirms that upgrades of commercial software should be checked prior to clinical use (Nisbet *et al*, 2004).

This work attempted to validate the entire treatment chain using a pelvic anthropomorphic phantom, fabricated using locally available materials as human tissue substitutes. The planning system used had two dose calculation algorithms, the PB and the CC. Both algorithms were used for clinical treatment planning. The plans showed that there was little or no clinically significant difference in the calculation of dose by the two algorithms however, no large non-unit density heterogeneity scenarios were studied. A limitation of the RTPS was the lack of interaction when the CC algorithm was used, for this reason, point doses were only obtained for the PB algorithm.

Thermoluminescent dosimetry is a relative dosimetry system and its accuracy depends on various parameters, such as the reproducibility of the TL reading, calibration techniques and efforts put into the measurement process. Most of the TLD results however were below the 10% dose deviation. For the 6 MV AP/PA field arrangement, 32 TLDs out of the total 35 TLDs exposed (91.4%) were below the 10% dose deviation, 40% (14/35) for the 6 MV four field arrangement, 91.4% (32/35) for the AP/PA field arrangement at 15 MV and 57.1% (20/35) for the four field arrangement at 15 MV. This result indicated that the TLD results were better at 15 MV than at 6 MV. The readings were reproducible

(standard deviations of less than 3) as shown in Tables A.1 – A.6. The absorbed dose rate of the treatment unit was confirmed with a calibrated ionization chamber before each of the TLD irradiations. The main source of uncertainty in this experiment could have been due to loss of signal due to fading caused by the heating cycle and TLD sensitivity to light. For this reason detectors should be shielded from light during use by, for example, a black polyethylene wrapper which can also serve to keep the detectors clean. Another source of uncertainties could have been due to variation in the treatment unit output as shown in figures 3.4 and 3.5. The supralinearity correction was not applied to the TLD readings as the point doses of interest in this study were within the linear region of TLD sensitivity. Three dose regions emerged for the four field "box" technique, those of low, intermediate and high dose gradient. TLDs placed in low dose gradients showed better agreement than those placed in high dose gradient regions. This was also observed by Kanduza (Kanduza, 2005).

The film calibration results obtained in this study gave sensitometric curves at 6 MV and 15 MV that almost overlapped, indicating energy independence of the film. The OD measured on the film after exposure was higher than doses predicted by the planning system and those measured at TLD dose points when a local cancer of the cervix protocol was used. However, when a smaller field size was employed, the OD was comparable to the TLD readings suggesting that the higher readings were mainly due to large field size placement. Over response of film is generally attributed to the softening of the photon spectra with depth in the phantom and also to the fact that the OD depends on many factors (e.g. photon energy, film plane orientation and processing conditions) the implication being that OD is not always associated with the same dose, making the conversion of OD to absolute dose a very difficult task. The conical design of the dosimetry insert restricts the size of film that can be used from 8 cm x 8 cm to 14 cm x 14 cm. The 70% isodose was therefore the minimum level visible on the largest films when the local cancer of the cervix protocol is followed (appendix A, figure A.1). The 2D isodose distributions obtained were therefore not meaningfully comparable to the ones predicted by the planning system or to the 2D isodoses obtained by Kanduza (Kanduza, 2005). Kanduza used field sizes of less than 12 x 12 cm for the dosimetry verification,

however this is not typical of cancer of the cervix field size placement. When a smaller field size was used (figure 3.15 and 3.16), the film results obtained were comparable to the TLD results (Table A.5 – A.6) even though both results were lower compared to doses predicted by the RTPS. Kanduza's methodology included the four field "box", AP/PA and arc therapy techniques at 6 MV and 10 MV. The verification between measured and calculated dose using TLDs in this study did not totally agree with that obtained by Kanduza. Comparisons of point doses could not be done as Kanduza did not indicate how the TLDs were positioned in the dosimetry insert. The results obtained by Kanduza using the AP/PA at 6 MV are shown in appendix B.

CONCLUSION AND RECOMMENDATIONS

The treatment planning system accurately predicted doses in the anthropomorphic phantom to within 3% of the prescribed dose at selected dose points as can be seen from Tables A.1 to A.6. However, the generally stated goal of dose delivery to an accuracy of within 5% was not met at most dose points, especially where the TLDs were placed in regions of high dose gradient.

The percentage dose deviation between dose measured by the TLDs and that calculated by the Helax planning system, was lower at 15 MV than at 6 MV.

- The TLD results at 6 MV photon beam energy obtained in this study did not totally agree with those obtained by Kanduza (Kanduza, 2005). The phantom was not found to be useful for 2D isodose distribution with film when the local cancer of the cervix protocol was employed. This was because the cut film dimensions were smaller than the set field size when this protocol was followed. Discrepancies between the results obtained in this study and those obtained by Kanduza with film dosimetry imply that the phantom is not suitable for film dosimetry of all beam arrangements. Nonetheless, the phantom could still be useful for dosimetry audits of techniques where the set field sizes are smaller than the film insert dimensions (e.g. 8 cm x 8 cm to 14 cm x 14 cm).

- The size of the TLD holes should be machined to accurately fit the dimensions of square TLD_100 chips to minimise systematic errors due to gaps and also prevent areas of non equilibrium. Alternatively, the holes could be machined to fit sachets of TLD powder.

- The sensitometric curves at 6 MV and 15 MV almost overlapped, indicating that the energy dependence of the film at these beam energies was minimal.

- The phantom is limited to film dosimetry of small field sizes.

- The phantom could be modified to incorporate bigger cylindrical inserts that would allow for more typical cancer of the cervix field size placement.

- A similar phantom that is affordable could be developed to accommodate an entire sheet of film in order to eliminate errors introduced by cutting the film.

- Provisions for reference ionization chamber measurements could serve as a means of accurately confirming the absolute dose.

- The decision to use either parallel or perpendicular irradiation for film calibration depends on the degree of energy dependence of the film used and the geometry that will be used for actual test measurements. The geometry used for the calibration of film should be the same as that used for actual measurement in the phantom. For this phantom, calibration of film should be carried out parallel.

- The Helax treatment planning system should be checked if it accurately corrects for electron density. The electron-density is the most important material property that should be taken into account by photon dose calculation algorithms and not the mass-density. The mass-density method tends to overestimate dose, relative to electron-density prediction.

REFERENCES

Ahnesjo, A. (1989) Collapsed Cone convolution of radiant energy for photon dose calculation in heterogeneous media. Med. Phys. **16** 577-592.

Ahnesjo, A. (1997) Cone discretization for the collapsed cone algorithm, *in proceeding of the int. conf on the use of computers in radiation therapy XII ICCR* Salt lake City, USA, edited by D. D Leavitt and G. Starkschall Medical Physics Publishing , Madison, WI 114-116.

Ahnesjo, A. (1994) Analytic modeling of photon scatter from flattening filters in photon therapy beans. Med. Phys. **21** 1227-1235.

Aspradakis, M.M., Morrison, R.H., Richmond, N.D. and Steele, A. (2003) Experimental verification of convolution/superposition photon dose calculation for radiotherapy treatment planning. Phys Med Biol. **48** 2873-2893.

Aspradakis, M. M., McCallum, H. M. and Wilson, N. (2006) Dosimetric and treatment planning considerations for radiotherapy of the chest wall. Br J Radiol. **79** 828-836.

Attix, F. H. (1986) Introduction to Radiological Physics and Radiation Dosimetry, Wiley, New York.

Bogucki,T. M., Murphy, W.R., Baker, C.W., Piaza, S.S and Haus, A.G. (1997) Processor quality control in laser imaging systems, Med. Phys. **24** 581-584.

Brahme, A. (1984) Dosimetric precision requirements in radiation therapy. Act Radiol Oncol **23** 379-391.

Burch, S.E., Yeo. I. J. and Wang, C.K. (1997) A new approach to film dosimetry for high energy photon beams: lateral scatter filtering. Med. Phys. **24** 773-783.

Cherry, P. and Duxbury, A. (1998) Practical Radiotherapy Physics and Equipment. Greenwich Medical Media. McGraw-Hill, New York, 2nd edition.

Cormack, A.M. (1963) Representation of a function by its line integrals, with some radiological application. J. App. Physics **34** 2722-2727.

Danclu, C., Proimos, B.S., Rosenwald, J and Mijnheer, B.J. (2001) Variation of sensitometric curves of radiographic films in high energy photon beams. Med. Phys. **28** (6) 966-974.

D'Angelo, L., Furetta, C., Giancola, S., Lannoli, D and Scaccol, A. (1999) Verification of treatment planning systems for therapeutic radiations using thermoluminescence dosimeters, Rad. Prot. Dos. **85** (4) 401-404.

Dunscombe, P., McGhee, P. and Lederer, E. (1996) Anthropomorphic phantom measurements for the validation of a treatment planning system. Phys. Med. Biol. **41** 399–411.

Dutreix, A., Blarngard, B.E., Bridier, A., Mijnheer, B., Shaw, J.E. and Svenson, H. (1997) Monitor unit calculation for high energy photon beams, ESTRO, booklet 3.

Ertl, A., Hart1, R.F., Zehetmayer, M., Kitz, K., Griffitt, W. (1996) TLD array for precise dose measurements in stereotactic radiation techniques Phys. Med. Biol. **41**(12) 2679-2686**.**

Fano, U. (1954) Note on the Bragg-gray cavity principle for measuring energy dissipation Radiat. Res. **1** 237-240.

Folkard, M., Roper, M.J. and Michael,B.D. (1989) Measurement and analysis of supralinearity in LiF TLD- 100 irradiated by 1.5 keV x-rays. Phys. Med. Biol. **34**(6), 707-715.

Fraass, B., Doppke, K., Hunt, M., Kutcher, G., Starkschall, G., Stem, R. and Van Dyke, J. (1998) American Association of Physicists in Medicine Radiation Therapy Committee Task group 53: Quality assurance for clinical radiotherapy treatment planning Med. Phys. **25** 1773–1829.

Hale, J.I., Kerr, T. and Shragge, P.C. (1994) Calibration of film for accurate megavoltage photon dosimetry, Med. Dosimetry **19** 43-46.

Helax-TMS 6.1B Manual, (2003), Dose formalism and models in helax-tms

Herrick, S. J. and Newman, D. F. (1999) Verification of a photon beam algorithm in a 3D radiation therapy treatment planning system. Med. Dosimetry **24** (3) 179-182.

ICRU Report 24, (1976) Determination of absorbed dose in a patient irradiated by beams of X or gamma rays, Washington DC.

ICRU Report 42, (1987) Use of computers in external radiotherapy procedures with high energy photons and electron, Washington D.C.

ICRU report 59, (1998) Clinical proton dosimetry part 1, beam production, beam delivery and measurement of absorbed dose. International commission on radiation and measurement . Bethusda M.D.

International Atomic Energy Agency, (2001) Absorbed dose determination in external beam therapy: An international code of practice for dosimetry based on absorbed dose to water. IAEA Technical Reports Series 398, Vienna.

Johns, H. E. and Cunningham, J. R. (1983) The physics of radiology, Fourth edition, 219-220, Thomas, Illinois.

Kanduza, M. (2005) Design and evaluation of a dosimetry system to verify the radiotherapy procedure from treatment planning to treatment delivery, MSc thesis, Pretoria University.

Karzmark, C.J. (1993) Medical Linear Accelerators, New York: McGraw Hill Inc

Khan, F.M. (2003) The Physics of Radiation Therapy 3rd ed. Philadelphia USA Lippincott Williams and Wilkins.

Knoos, T., Ceberg, C., Weber, L. and Nilson. P. (1994) "The dosimetric verification of a pencil beam based treatment planning system. Phys. Med. Biol. **39** 1609-1628.

Knoos, T. Ceberg, C., Weber, L. and Nilson. P. (1995) Limitations of a pencil beam approach to photon dose calculation in lung tissue. Phys. Med. Biol. **40** 1411-1420.

Leszczynski, K.W. and Dunscombe, P.B. (2000) Independent corroboration of monitor unit calculations performed by 3D computerized planning system. J. App Clin Med Phys, **1**, (4) 234-242.

Mayles, W. P.M., Heisig, S. and Mayles, H.M.O. (1993) Treatment verification and in vivo dosimetry. Radiotherapy Physics in Practice, Oxford University Press, Oxford.

Meigooni, S. A., Mishra, V., Panth, H. and Williamson, J. (1995) Instrumentation and dosimeter size artifacts in quantitative thermoluminescence dosimetry of low dose fields, Med. Phys. **22** 555-561.

Metcalfe, P., Kron, T. and Hoban, P. (1997) The Physics of Radiotherapy X-Rays from Linear Accelerators. Madison, WI: Medical Physics Publishing.

Mijnheer, B.J., Battermann, J.J. and Wambersie, A. (1987) What degree of accuracy is required and can be achieved in photon and neutron therapy? *Radiother. Oncol.* **8** 237–252.

Mihailidis, D.N., Alkhatib,H., Gibbons, J.P. (2000). Use of primary off-axis ratios for dose and monitor unit calculation in wedged photon beams with asymmetric collimation. **2** 1088-1091.

Moller, T.R., Ceberg, J., Eimham, N., Lindholm, C. and Nylen, U. (2003) Radiotherapy techniques in current use in Sweden. Act Oncologica **42**, (5/6) 376-386.

Newman, D.L, Dougherty, G.A.l., Obaid, A. and Hajrasy, H.A.l. (1998) Limitations of CT in assessing cortical thickness and density, Phys. Med. Biol. **43** 619–626.

Nilsson, M. and Knoos,T. (1992) "Application of the Fano theorem in inhomogeneous media using a convolution algorithm," *Phys. Med. Biol*. **37** 69–83.

Nisbet, A., Beange, I., Vollmar, H., Irvine, C., Morgan, A and Thwaities D.I. (2004) Dosimetric verification of a commercial collapsed cone algorithm in simulated clinical situations. Radiotherapy and oncology **73** 79-88

Novotny, J., Gomola, I., Izewska, J. and Huyskens, D. (1997) External audit of photon beams by mailed film dosimetry: feasilibility study. Phys. Med. Biol. **42** 1277-1288

O'Connor, J.E. (1957) The variation of scattered x-rays with density in an irradiated body Phys. Med Biol **1** 352-369

Pai, S., Das, I.J., Dempsey, J.F., Lam, K.L., LoSasso, J.T., Olch, J.A., Palta, J.R., Reinstein, L.E., Ritt, D and Wilcox, E.E. (2007) Radiographic film for mega voltage beam dosimetry, Med Phys **34** (6) 2228-2258

Papinikalaou, N., Battista, J.J., Boyer, A.L,. Kappas, C., Klein, E., Mackie, T.R., Sharpe, M. and Van Dyk, J (2004) Tissue inhomogeneity correction for megavoltage photon beams. Report of Task Group No 65 of the Radiation Therapy Committee of the American Association of Physicists in Medicine. Medical Physics Publishing.

Starkschall, G., Steadham, R.E., Wells, N.H., O'Neil, L., Miller, L.A and Rosen, I.I. (2000) On the need for monitor unit calculations as part of a beam commissioning methodology for a radiation treatment planning system. J. Appl. Clin. Med.Phys. **1** 86-94

Suchowerska, N., Hoban, P., Davison, A. and Metcalfe, P. (1999) "Perturbation of radiotherapy beams by radiographic film: measurements and Monte Carlo simulations," Phys. Med. Biol. **44** 1755–1765

Swinnen, A. (2005) Quality assurance in radiotherapy: Development and validation of a mailed dosimetry procedure for external audits using a multipurpose phantom and in vivo dosimetry. PhD Thesis Katholieke University Leuven

Weber, L. and Nilsson, P. (2002) Verification of dose calculations with a clinical treatment planning system based on a point kernel dose engine. J.Appl Clin Med Phys, **3** 73-87

Yeo, I.J., Wang, C.K. and Bursch, S.E. (1999). A new approach to film dosimetry for high energy photon beams using organic plastic scintillators. Phys. Med. Biol. **44** 3055-3069.

Yu, C. and Luxton, G. (1999) TLD dose measurement: A simplified accurate technique for the dose range from 0.5 cGy to 1000 cGy. Med Phys. **26** (6) 1010-1016

Zimmerman, D. W., Rhyner, C.R. and Cameron, J.R. (1966) Thermal annealing effects on the thermoluminescence of LiF, Health physics **12** 525-531

APPENDIX A

Table A.1 Individual TLD results for 6 MV AP/PA compared to point doses predicted by the planning system when the local cancer of the cervix protocol is used.

TLD Identification	Average measured dose (cGy)	Expected dose (cGy) (PB)	% Dose deviation
A5	67.8 ± 0.4	73.5	*8.5*
A6	68.6 ± 0.2	73.5	*7.2*
A7	70.1 ± 1.3	72.1	*2.9*
A8	68.4 ± 2.5	72.1	*5.5*
A9	66.6 ± 0.4	70.7	*6.2*
B1	62.6 ± 0.6	70.0	*11.8*
B2	69.3 ± 0.4	73.5	*6.1*
B3	68.5 ± 2.3	74.2	*8.3*
B4	71.6 ± 2.5	73.5	*2.7*
B5	66.7 ± 1.9	72.1	*8.2*
B6	66.9 ± 0.2	72.1	*7.9*
B7	65.9 ± 0.5	71.4	*8.4*
B8	63.8 ± 1.8	70.7	*10.8*
B9	69.5 ± 3.0	73.5	*5.8*
C1	67.8 ± 0.4	74.2	*9.4*
C2	69.1 ± 2.3	73.5	*6.4*
C3	66.1 ± 0.8	72.1	*9.1*
C4	65.8 ± 1.1	72.1	*9.6*
C5	64.1 ± 0.1	71.4	*11.4*
C6	65.4 ± 0.4	70.7	*8.1*
C7	69.9 ± 0.1	74.2	*6.2*
C8	72.0 ± 1.5	74.9	*4.1*
C9	69.4 ± 1.2	72.8	*5.0*
D1	67.6 ± 0.6	72.1	*6.7*
D2	68.7 ± 0.5	72.1	*5.0*
D3	68.5 ± 0.8	72.8	*6.4*
D4	68.5 ± 0.7	71.4	*4.2*
D5	69.7 ± 0.4	74.9	*7.5*
D6	70.2 ± 1.1	74.2	*5.8*
D7	67.3 ± 0.1	72.8	*8.2*
D8	66.0 ± 1.0	70.7	*7.1*
D9	66.7 ± 2.4	71.4	*7.0*
E1	67.4 ± 1.8	72.1	*7.0*
E2	65.6 ± 2.0	71.4	*8.8*
E3	68.3 ± 0.2	74.2	*8.7*

Table A.2 Individual TLD results for 6 MV Four Field "box" compared to point doses predicted by the planning system when the local cancer of the cervix protocol is used.

TLD Identification	Average measured dose (cGy)	Expected dose (cGy) (PB)	% Dose deviation
A5	45.6 ± 1.3	53.2	*16.9*
A6	46.4 ± 1.3	53.2	*14.9*
A7	46.9 ± 0.7	53.9	*14.9*
A8	47.7 ± 0.7	63	*32.1*
A9	64.0 ±3 .5	72.8	*13.8*
B1	60.8 ± 0.9	73.5	*21.0*
B2	45.6 ± 0.3	53.2	*16.7*
B3	48.0 ± 0.8	52.5	*9.5*
B4	47.8 ± 0.5	53.2	*11.4*
B5	47.9 ± 0.6	53.2	*11.1*
B6	49.5 ± 1.1	61.6	*24.6*
B7	63.5 ± 1.2	70.7	*11.4*
B8	62.6 ± 0.4	70.7	*13.0*
B9	45.9 ± 0.1	52.5	*14.4*
C1	47.1 ± 0.4	53.2	*13.0*
C2	46.0 ± 1.8	53.2	*15.8*
C3	49.5 ± 0.4	53.2	*7.5*
C4	48.5 ± 0.4	60.2	*24.3*
C5	62.1 ± 0.4	70.7	*13.9*
C6	63.6 ± 1.0	70.7	*11.2*
C7	49.2 ± 0.9	52.5	*6.8*
C8	49.9 ± 0.6	53.2	*6.7*
C9	50.7 ± 1.3	53.2	*4.9*
D1	49.7 ± 0.1	53.2	*7.0*
D2	50.5 ± 0.1	61.6	*22.1*
D3	66.8 ± 1.1	72.1	*7.9*
D4	67.5 ± 0.8	71.4	*5.8*
D5	50.0 ± 0.6	53.2	*6.5*
D6	50.3 ± 0.1	53.9	*7.2*
D7	48.9 ± 0.3	53.2	*8.8*
D8	50.0 ± 0.1	61.6	*23.2*
D9	65.4 ± 0.1	71.4	*9.2*
E1	64.6 ± 2.7	71.4	*10.5*
E2	67.3 ± 1.3	71.4	*6.2*
E3	50.6 ± 0.4	53.9	*6.6*

Table A.3 Individual TLD results for 15 MV AP/PA compared to point doses predicted by the planning system when the local cancer of the cervix protocol is used.

TLD Identification	Average measured dose (cGy)	Expected Dose (cGy) (PB)	% Dose deviation
A06	64.9 ± 0.4	71.54	*9.3*
A07	63.8 ± 0.9	72.24	*11.8*
A08	66.7 ± 0.3	71.82	*7.1*
A09	65.5 ± 0.9	71.26	*8.2*
B01	65.9 ± 0.1	70.21	*6.1*
B02	65.9 ± 0.8	69.93	*5.8*
B03	65.7 ± 0.5	71.54	*8.2*
B04	67.6 ± 0.2	72.24	*6.5*
B05	66.0 ± 0.4	72.59	*9.1*
B06	65.1 ± 0.1	71.75	*9.3*
B07	66.3 ± 0.6	71.82	*7.8*
B08	65.5 ± 0.5	70.91	*7.7*
B09	66.4 ± 1.1	70.56	*6.0*
C01	66.8 ± 1.1	72.1	*7.4*
C02	68.0 ± 1.2	72.59	*6.4*
C03	66.7 ± 0.4	73.01	*8.6*
C04	63.6 ± 1.1	71.82	*11.5*
C05	66.7 ± 0.2	71.89	*7.3*
C06	67.3 ± 1.1	71.4	*5.7*
C07	68.0 ± 0.6	70.91	*4.2*
C08	70.1 ± 1.1	72.59	*3.4*
C09	69.5 ± 0.9	73.01	*4.9*
D01	66.7 ± 1.7	72.31	*7.8*
D02	66.3 ± 0.3	71.12	*6.8*
D03	65.0 ± 0.1	71.68	*9.4*
D04	70.2 ± 1.0	72.17	*2.7*
D05	68.5 ± 0.8	71.54	*4.3*
D06	68.4 ± 0.3	72.17	*5.2*
D07	70.8 ± 1.8	72.94	*2.9*
D08	65.9 ± 2.8	72.31	*8.9*
D09	63.5 ± 2.1	70.7	*10.3*
E01	71.2 ± 1.1	71.05	*0.2*
E02	71.6 ± 1.2	72.03	*0.7*
E03	72.9 ± 1.2	71.54	*1.8*
E04	72.7 ± 0.4	73.01	*0.4*

Table A.4 Individual TLD results for 15 MV four field "box" compared to point doses predicted by the planning system when the local cancer of the cervix protocol is used.

TLD Identification	Average measured dose (cGy)	Expected dose (cGy) (PB)	% Dose deviation
A06	43.30 ± 2.8	49.21	*12.0*
A07	43.85 ± 0.8	50.26	*12.8*
A08	46.75 ± 1.5	51.10	*8.5*
A09	48.85 ± 0.6	61.53	*20.6*
B01	62.85 ± 0.1	71.68	*12.3*
B02	65.80 ± 1.1	72.17	*8.8*
B03	44.55 ± 0.1	49.70	*10.4*
B04	44.50 ± 0.3	49.07	*9.3*
B05	45.05 ± 0.4	50.19	*10.2*
B06	45.70 ± 0.4	51.17	*10.7*
B07	51.40	62.09	*17.2*
B08	64.95 ± 0.9	70.21	*7.5*
B09	67.60 ± 1.1	70.84	*4.6*
C01	43.80 ± 0.3	49.07	*10.7*
C02	44.50 ± 0.3	49.07	*9.3*
C03	45.55 ± 0.6	50.19	*9.2*
C04	45.40 ± 0.8	50.82	*10.7*
F01	49.55 ± 1.2	59.99	*17.4*
C06	65.35 ± 0.9	70.28	*7.0*
C07	67.55 ± 0.1	70.56	*4.3*
C08	46.95 ± 0.4	49.00	*4.2*
C09	46.95 ± 0.4	49.91	*5.9*
D01	44.40 ± 0.7	49.98	*11.2*
D02	45.75 ± 0.1	50.47	*9.4*
D03	48.75 ± 1.3	59.01	*17.4*
D04	70.10 ± 1.4	71.19	*1.5*
D05	67.75 ± 1.3	71.26	*4.9*
D06	44.75 ± 0.8	49.00	*8.7*
D07	48.10 ± 1.0	50.40	*4.6*
D08	46.00 ± 1.0	51.38	*10.5*
D09	47.90 ± 1.8	57.68	*17.0*
E01	69.00 ± 0.4	70.28	*1.8*
E02	69.70 ± 1.0	71.54	*2.6*
E03	70.25 ± 0.2	71.40	*1.6*
E04	49.15 ± 1.5	50.54	*2.8*

Table A.5 Individual TLD and film results for 6 MV AP/PA treatment plan based on figure 4.9 compared to point doses predicted by the planning system.

TLD Identification	Average) (cGy)	Expected Dose (cGy)	% Dose Deviation (TLD)	Optical Density	Corresponding Dose on film (cGy)
A20	63.3±0,2	74.5	*17.8*	2.57	64
A50	68.5±0.3	74.3	*8.5*	2.64	67
A60	64.8±0.1	74.2	*14.5*	2.69	68
A70	68.5±0.7	73.5	*7.3*	2.59	66
A80	64.8±0.1	73.5	*13.5*	2.69	68
A90	63.9±0.3	73.5	*15.0*	2.72	70
B10	68.5±0.4	72.5	*5.6*	2.59	66
B20	62.7±0.8	72.7	*16.1*	2.71	70
B30	63.2±0.9	73.5	*16.3*	2.72	70
B40	61.7±1.4	71.7	*16.3*	2.58	66
B50	65.3±1.3	72.0	*10.2*	2.7	69
B70	64.5±0.3	71.9	*11.5*	2.76	71
C20	62.6±0.2	71.1	*13.7*	2.61	67
C30	65.7±0.7	71.5	*8.9*	2.69	69
C50	64.5±1.3	71.9	*11.5*	2.76	71

Table A.6 Individual TLD and film results for 6 MV four field "box" treatment plan based on figure 4.10 compared to point doses predicted by the planning system.

TLD Identification	Average) (cGy)	Expected Dose (cGy)	% Dose Deviation (TLD)	Optical Density	Corresponding Dose (film) (cGy)
D10	47.4±0.6	46.2	*-2.5*	2.03	46
D20	41.0±2.8	46.2	*12.7*	2.02	46
D30	41.2±0.3	46.2	*12.1*	1.93	42
D40	43.7±0.8	46.2	*5.8*	2.02	44
D60	42.8±0.6	46.2	*7.9*	2.02	44
D70	48.1±0.2	46.2	*-3.9*	1.97	45
D80	44.5±1.6	49.0	*10.2*	2.09	47
E10	45.4±0.6	48.3	*6.5*	2.06	46
E20	45.0±0.8	49.7	*10.4*	2.05	46
E30	62.8±0.1	69.3	*10.4*	2.62	66
E40	68.7±0.2	69.3	*0.9*	2.62	66
E50	65.4±0.1	70.7	*8.2*	2.57	63
E60	71.3±0.4	71.4	*0.2*	2.63	67
E80	67.5±0.2	71.4	*5.9*	2.65	67
F10	64.3	71.4	*11.0*	2.55	63

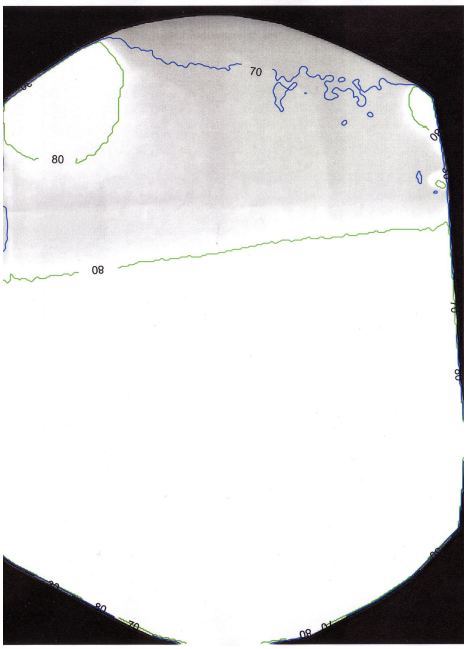


Figure A.1 2-D isodose distribution at 15 MV for the four field box technique using a local cancer of the cervix protocol. Film was cut and positioned as shown in figure 4.5



Figure A.2 Shows an exposed film (using a 7 cm x 7 cm field size) at 6 MV for the four field box technique, showing the box shape. Film was cut and positioned in figure 4.10.

APPENDIX B

Table B.1This table shows Kanduza's TLD results at 6 MV using the AP/PA technique. A field size of 10 cm x 10 cm was used (Kanduza, 2005).

Measured and calculated interest point doses.

Anterior-posterior/Posterior-anterior

calculated dose	measured dose	% difference
68.1	70.7	-3.817914831
68.2	67.6	0.879765396
67.6	70.6	-4.437869822
67.7	71.7	-5.908419498
67.2	72.7	-8.18452381
67.2	66.2	1.488095238
67.8	76.8	-13.27433628
67.8	73.1	-7.817109145
67.2	68.4	-1.785714286
67.1	68.6	-2.235469449
68.1	70.5	-3.524229075
68	72	-5.882352941
67.8	71.4	-5.309734513
68.4	71.5	-4.532163743
65.7	72.6	-10.50228311
65.9	69.7	-5.766312595
65.9	70.9	-7.587253414
66.2	67.7	-2.265861027
66.8	69.6	-4.191616766
66.4	66.4	0
66.2	67.5	-1.963746224
67.3	73.7	-9.509658247
64.9	69.1	-6.471494607
64.8	67.1	-3.549382716
64.7	67.6	-4.482225657
65.3	67.8	-3.82848392
66.4	66.4	0
63	66	-4.761904762
64.7	68.4	-5.7187017
64.2	61.9	3.582554517
63.6	66.4	-4.402515723

Calculated	Measured	% difference
63.9	61.7	3.442879499
63.8	64	-0.313479624
64.7	65.7	-1.545595054
63.7	65.8	-3.296703297
64.7	71.2	-10.04636785
64.1	66	-2.964118565
63.2	64.8	-2.53164557
64	66.2	-3.4375
63.6	67.7	-6.446540881
62.8	63.4	-0.955414013
63.6	66.4	-4.402515723
61.3	62.8	-2.446982055
65.2	45.3	30.52147239
59.7	55.7	6.700167504
63.9	63.4	0.782472613
63.8	42.7	33.07210031
59.3	58	2.192242833
62.8	46	26.75159236
58.9	62.3	-5.772495756
65.5	64.3	1.832061069
64.7	59.5	8.037094281
59.1	57.2	3.214890017
63.8	60.2	5.642633229
67.7	59.9	11.52141802
67.5	65.4	3.111111111
56.3	53.4	5.150976909
65.6	66.3	-1.067073171
64.3	56.2	12.59720062
64.9	64.1	1.232665639
64.7	63.9	1.236476043
66.7	67.5	-1.1994003
66.2	70.1	-5.891238671
66.1	70.2	-6.202723147
66.1	69.8	-5.597579425
65.6	68.7	-4.725609756